Experimental investigation on the tensile behaviour of welded RHS high strength steel X-joints

Yan, R.; Mela, Kristo; El Bamby, H.; Veljkovic, M.

DOI
10.1016/j.engstruct.2022.115357

Publication date
2023

Document Version
Final published version

Published in
Engineering Structures

Engineering Structures 276 (2023) 115357

Contents lists available at ScienceDirect

Engineering Structures

journal homepage: www.elsevier.com/locate/engstruct

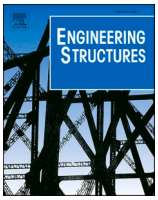

Experimental investigation on the tensile behaviour of welded RHS high strength steel X-joints

Rui Yan [a,*], Kristo Mela [b], Hagar El Bamby [a], Milan Veljkovic [a]

[a] Department of Engineering Structures, Delft University of Technology, Delft, the Netherlands
[b] Faculty of Built Environment, Tampere University, Tampere, Finland

ARTICLE INFO

Keywords:
Welded tubular joints
High strength steel
Cold-formed rectangular hollow section
X-joint

ABSTRACT

The newest version of prEN 1993-1-8 (2022) prescribes a material factor (C_f) to reduce the design resistance of welded joints made of high strength steel (HSS) mostly due to the lack of available experiments, given the less ductility of HSS compared to mild steel. Additionally, it is stated that the material design yield strength should not exceed 0.8 times the ultimate strength (f_u) for the chord punching shear failure and the tensile brace failure. The mechanical background behind C_f and the $0.8f_u$ restriction for different types of joints and loading conditions is vague. In this paper, the validity of C_f and the $0.8f_u$ restriction is investigated experimentally by considering 18 welded rectangular hollow section X-joints tested in tension. A bi-linear model, which is suitable for an elasto-plastic global analysis considering the post-yielding stiffness, is proposed to characterize the nonlinear behaviour of the joint. The predicted resistance and failure mode, with and without considering the C_f and/or the $0.8f_u$ restriction, are compared to the experimental results. In addition, the predicted resistance corresponding to the experimental failure mode is investigated. It is concluded, based on the tested joints in this paper and literature, that C_f and the $0.8f_u$ restriction are not necessary for the design according to prEN1993-1-8. However, the predicted brace failure resistance is unconservative for tested joints that failed by brace failure if C_f for S700 or the $0.8f_u$ restriction for all steel grades is not considered.

1. Introduction

Welded joints between tubular members are often used in trusses and building frames, bridges, and off-shore structures. In Europe, welded tubular joints are designed according to the approved standard EN 1993-1-8 (2005) [1], which presents a series of design rules that take into account the configuration of the joint, and the various failure modes that have been identified in research. These rules have been developed based on extensive experimental and numerical investigations on joints made of mild steel (S235 and S355) before 2005. To allow using steel grades higher than S355, a material factor ($C_f = 0.9$) for reducing the design resistance has been stipulated for joints using materials higher than S355 and up to S460 [1].

Due to advanced material manufacturing techniques, such as Thermo-mechanical control process (TMCP) and Quenching & Tempering (QT), high strength steel (HSS) hollow sections (460 MPa $< f_y \leq$ 700 MPa) have become more readily available in recent years. HSS has higher strength, but lower ductility compared to mild steel. The size of structural members can be effectively reduced using HSS, resulting in a lower self-weight, less welding because of thinner profiles, and consequently, substantial economic and environmental benefits. A very good practical example of considerable cost saving was accomplished in the Friends Arena in Stockholm [2], where HSS (S460, S690, and S900) hollow sections and other profiles were used for the roof of the stadium. The financial cost and greenhouse gas emissions were reduced by 14.5 % and 17 %, respectively, compared to the mild steel design.

Regarding the design of HSS welded tubular joints, EN 1993–1-12 [3] provides supplementary rules for EN 1993–1–8 [1], extending the range of steel grades up to S700. The general approach of EN 1993–1-12 [3] is that HSS welded tubular joints are designed by the same expressions as joints of mild steels, and the material factor ($C_f = 0.8$ for 460 MPa $< f_y \leq$ 700 MPa steels) is applied to the obtained resistance. In the latest version of prEN1993-1–8 [4], C_f was increased from 0.8 to 0.86 for 460 MPa $< f_y \leq$ 550 MPa materials. In addition, a material ductility restriction on the yield strength (f_y) was imposed for punching shear failure (PSF) and tension brace failure (BF), stating that in design, the value of the yield strength should be limited to 0.8 times the ultimate strength (f_u). However, applying C_f and the $0.8f_u$ restriction partially

* Corresponding author.
E-mail address: r.yan@tudelft.nl (R. Yan).

https://doi.org/10.1016/j.engstruct.2022.115357
Received 13 July 2022; Received in revised form 27 October 2022; Accepted 22 November 2022
Available online 8 December 2022

eliminates the benefits of using HSS, limiting its competitiveness.

Justifications of C_f were based on experimental and numerical studies on gap K-joints [5–8]. However, the mechanical background behind C_f for different types of joints and loading conditions is vague. For PSF and BF in HSS joints, the fracture occurs in the heat-affect zone (HAZ), whose mechanical properties are heavily influenced by the parameters of the welding process, such as the heat input, the cooling time, the welding technique [9,10], and mechanical properties of hollow section (the base) material. In general, the higher the steel grade is followed by the more severe the HAZ strength reduction [10–12]. Javidan et al. [13] found an approximate 30 % strength reduction in S960 HAZ compared to the base material. A 15 % ultimate strength reduction in S700 HAZ was reported by Yan et al. [11], while a limited strength reduction was observed in S700 HAZ using the laser welding technique [10]. Although BF and PSF are closely related to the HAZ strength, the HAZ material softening, especially for HSS, has not been explicitly considered in prEN1993-1–8 [4]. In the latest discussion regarding prEN1993-1–12 [14], the HAZ strength deterioration in ultra-high strength steel (UHSS) with steel grade above S700 is recognized as one of the important research questions.

In the last decade, many investigations have been carried out on HSS X-joints in tension [12,15–17]. Feldmann et al. [12] found that no reduction was needed for S500 joints, but a 0.9 and 0.8 reduction factor was necessary for S700 and S960 joints, respectively. This conclusion was drawn based on 106 RHS X- and K-joints tension and compression tests. The original report did not distinguish C_f for the different types of joints and loading conditions. Regardless of the weld thickness, the tensile tests of X-joints demonstrate that design rules could safely predict the resistance without considering C_f and the $0.8f_u$ restriction for S500 and S700 joints but not S960 joints. It is worth mentioning that some X-joints were made with a single welding pass (nominal thickness varying from 3 mm to 5 mm). The tensile behaviour of X-joints was investigated at −40 °C (S420) [15] and the ambient temperature (S420 and S460) [16]. It was found that the −40 °C temperature did not influence the joint resistance and the deformation capacity. Becque and Wilkinson [17] carried out tension and compression tests on 4 T- and 11 X-joints made of C450 RHS. It was concluded that C_f (0.9) was required for PSF and BF. The conclusions were drawn considering a safety factor, $\gamma = 1.25$ for brittle failure modes and $\gamma = 1$ for ductile failure modes. Such distinction is not included in EN1993-1–8 [1]. However, based on the presented data, it is found that the predicted resistance without considering C_f and the $0.8f_u$ restriction is lower than the experiments. The material factor was re-evaluated for the chord side wall failure (CSWF) and BF by Wardenier et al. [18]. An equation was proposed to correlate the steel grade and the material factor.

In recent years, extensive experimental and numerical investigations on HSS and UHSS tubular X- and *T*-joints in compression and bending have been carried out [19–25]. Lee et al. [24,25] investigated the compressive behaviour of cold-formed mild steel and HSS CHS X-joints based on 9 tests. C_f for CFF was too conservative, and the joint strength equations were less conservative for joints with small β (the brace-to-chord ratio), which was confirmed by Lan et al [22,23]. Pandey and Young [19,21] investigated the compression capacity of welded cold-formed UHSS (S900 and S960) *T*-joints. It was concluded that the design rules overestimated the resistance of joints with small β. However, the equal-width ($\beta = 1$) joint resistance was significantly underestimated, which was also reported by Kim et al. [20]. Hence, the material factor was required for joints with small β but not equal-width joints. Havula et al. [26] found that the weld type and thickness significantly influenced the joint resistance and stiffness, which was also reported in [12,15,16].

All the above-mentioned experimental study is summarized in Table 1. Note that the information in the "Conclusions" and "Comments" columns are from the original paper and a re-evaluation of this study, respectively, based on the presented experimental data. It can be seen that the available tensile tests on cold-formed RHS X-joints with material

Table 1
Summary of the literature review.

References	Joints	Shape	Steel grade	Load	Note	Conclusions	Comments
Björk and Saastamoinen, 2012 [15]	20 X-joints	RHS	S420MH (S355J2H)	Tension	−40 °C, cold-formed tubes, 1.03 ~ 1.62 t_1 fillet weld	C_f is not necessary.	Both C_f and $0.8f_u$ are not necessary.
Feldmann et al., 2016 [12]	68 X- and 38 K-joints	RHS	S500, S700, S960	Tension and compression	Cold-formed and hot-finished tubes, 0.69 ~ 1.57 t_1 fillet weld	C_f is necessary for S700 and S960 but not S500 joints.	Both C_f and $0.8f_u$ are not necessary for S500 and S700 X-joints in tension.
Tuominen and Björk, 2017 [16]	20 X- and 10 K- joint	RHS	S420, S460	Tension and compression	Cold-formed and hot-finished tubes, 1.0 t_1 single bevel butt weld and 1.04 ~ 1.45 t_1 fillet weld	C_f is not necessary.	Both C_f and $0.8f_u$ are not necessary for X-joints in tension.
Becque and Wilkinson, 2017 [17]	4 T- and 11 X-joints	RHS	C450 (f_{yn} = 450 MPa)	Tension and compression	Cold-formed tubes, single bevel butt weld + 0.5 t_1 fillet weld, $\gamma = 1.25$ for PSF and BF considered	C_f is necessary for PSF and BF but not CFF and the side wall buckling.	Both C_f and $0.8f_u$ are not necessary for X-joints in tension.
Lee et al., 2017 [24], 2018 [25]	9 X-joints	CHS	SM490 (f_{yn} = 325 MPa), SM570 (f_{yn} = 420 MPa), HSA800 (f_{yn} = 650 MPa)	Compression	Cold-formed tubes, single bevel butt weld + fillet weld	C_f (0.8) is too conservative.	
Kim et al., 2019 [20]	6 X-joints	RHS	SM490 (f_{yn} = 325 MPa), HSA800 (f_{yn} = 650 MPa)	Compression	Cold-formed channel tubes, single bevel butt weld	C_f is not necessary.	
Pandey and Young, 2019 [19], 2020 [21]	22 T- and 34 X-joints	CHS & RHS	S900, S960	Compression	Cold-formed tubes, 0.97 ~ 1.81 t_1 fillet weld	C_f is necessary for all joints but not the equal-width ($\beta = 1$) joint	
Lan et al., 2019 [22], 2021 [23]	8 X- and 7 *T*-joints	CHS & RHS	Q890 (f_{yn} = 890 MPa)	Compression	Built-up tubes, 0.77 ~ 1.0 t_1 fillet weld	New C_f was proposed. Conservative prediction for large β.	
Havula et al., 2018 [26]	20 *T*-joints	RHS	S420, S500, S700	Bending	Cold-formed tubes, single bevel butt weld, 0.75 t_1 fillet weld, 1.25 t_1 fillet weld	C_f is necessary for all butt weld joints and S700 joints with 0.75 t_1 fillet weld.	

above S460 are still quite limited. Therefore, in this study, the results of 18 tensile tests on welded RHS X-joints made of mild steel and HSS are reported and analysed. The aim of the research is to examine the validity of C_f and the $0.8f_u$ restriction. The predicted failure modes are compared to the experimental failure modes. Additionally, a bi-linear model, suitable for an elasto-plastic global analysis considering the post-yielding stiffness, is proposed to characterize the nonlinear behaviour of the joint. It is concluded that C_f and the $0.8f_u$ restriction are not necessary for the resistance prediction of tested joints in this paper and literature, using prEN1993-1–8 [4]. However, the predicted BF resistance is too optimistic for tested joints that failed in the brace if C_f for S700 or the $0.8f_u$ restriction for all steel grades is not considered.

2. Experiments

2.1. X-joint tensile tests

Consider a welded tubular X-joint consisting of two braces and a chord, as shown in Fig. 1. The braces are welded to the opposite surfaces of the chord such that the joint is symmetric. A tensile load is applied to the braces.

The tested X-joints were made of three steel grades, namely S355, S500, and S700. S355 represents a reference case to which the HSS grades are compared. Specimens for each steel grade included three configurations with various brace width to chord width ratios (β). The main purpose for selecting three β values is to test joints with different deformation capacities and failure modes, as β governs the failure mode according to prEN 1993–1-8 [4]. Given the welding quality of different companies, two Dutch workshops, proficient in welding HSS, (Company A and B) were employed to fabricate 9 joints each, resulting in 18 joints in total. The nominal and measured dimensions of each joint are presented in Appendix A and Table 2, respectively. The symbols "A" and "B" represent the specimens fabricated by Company A and Company B, respectively. The nominal RHS dimensions for each joint were identical between Company A and B, except for the chord of XS500A/B1, XS700A/B2, and XS700A/B3. The length of the chord and the brace was 1.5 m and 0.4 m, respectively. The outer radius for nominal 4 mm, 5 mm, 6 mm, 8 mm, and 10 mm tubes were 8.5 mm, 9 mm, 13 mm, 20 mm, and 25 mm, respectively. Note the chord of XS500B1 and the brace of XS700A/B1 had the h_0/b_0 ratio of 0.45 and 3, respectively, which were beyond the stipulated limit (0.5 to 2). Additionally, $\beta = 0.25$ for XS355A/B1 is below the required minimum value $0.1 + 0.01b_0/t_0 = 0.35$, according to the range of validity for welded joints [4].

The brace was welded to the chord with a full-penetration butt weld. A single-bevel groove was produced in the brace before welding. A butt weld typically consists of three types of welding pass: the root (pass 1), the fill (passes 2 and 3), and the cap (passes 4 and 5), as shown in Fig. 1. The cap pass results in an extra fillet weld, making the whole weld thicker than the parent plate. Therefore, the throat thickness (a) of the fillet weld was measured. Note that the throat thickness is not applicable on Side A (see Fig. 1) of the joint with a large β value. The average throat thickness is presented in Table 2.

Company A used the filler metal Carbofil 1 to weld S355 tubes, while the filler metal Union Nimocr welded S500 and S700 tubes. Company B used the filler metal MEGAFIL 710 M for S355 and S500 joints and MEGAFIL 742 M for S700 joints. Both companies used the metal active gas (MAG) welding process. The minimum preheated temperature, the maximum interpass temperature, the heat input, and the mechanical property of filler metal for each steel grade are presented in Table 3. The main reason for employing two welding companies instead of carrying out the welding in laboratory conditions was to get test specimens welded with current industry practices and quality control. The welding companies provided some data from their Welding Procedure Specification (WPS) as presented in Table 3. However, more detailed data of the welding process was not obtained for this study.

The X-joints were tested in a setup with 2 MN capacity (Fig. 2 a)), except for 8 X-joints X355A/B2, X355A/B3, X500A/B2, and X500A/B3, which were tested in a 10 MN setup (Fig. 2 b)). A constant loading rate of 0.01 mm/s was used during the whole testing process. For the joint XS355A/B1, the loading rate was changed to 0.1 mm/s at the plastic stage as a significant deformation appeared. All joints were tested until the final failure with an obvious fracture and a sudden load drop.

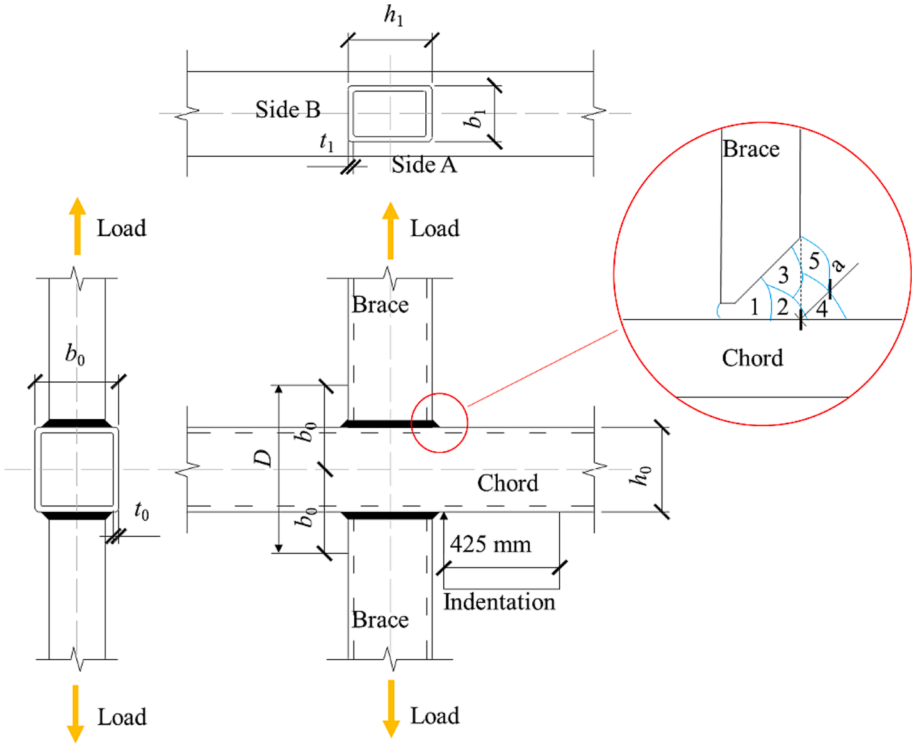

Fig. 1. Schematic of an X-joint.

Table 2
Measured geometric property of X-joints. (See Fig. 1 for the definition of dimensions.).

Specimen	Steel grade	b_0 [mm]	h_0 [mm]	t_0 [mm]	b_1 [mm]	h_1 [mm]	t_1 [mm]	β	a_{sideA} [mm]	a_{sideB} [mm]
XS355A1	S355	199.0	100.4	7.9	50.2	100.3	5.0	0.25	5.1	5.3
XS355A2		159.6	160.5	10.0	140.1	139.6	8.3	0.88	–	6.2
XS355A3		150.5	149.9	6.1	149.9	150.4	6.0	1	–	5.4
XS500A1	S500	200.0	101.1	7.9	90.5	159.9	7.9	0.45	6.6	6.6
XS500A2		160.9	160.8	9.8	140.4	140.4	7.9	0.87	–	8.6
XS500A3		150.7	150.2	6.0	150.5	150.3	6.0	1	–	5.1
XS700A1	S700	120.4	120.3	7.9	51.0	153.2	6.0	0.42	6.3	6.2
XS700A2		161.5	160.5	9.9	80.5	100.7	4.1	0.5	5.5	5.6
XS700A3		139.9	140.4	5.9	120.6	80.4	6.0	0.86	–	5.4
XS355B1	S355	199.9	101.0	8.1	50.5	100.0	5.1	0.25	5.9	5.1
XS355B2		160.5	160.5	10.0	140.1	140.1	8.1	0.87	–	7.5
XS355B3		150.5	151.0	6.2	150.8	150.8	6.2	1	–	7.7
XS500B1	S500	180.5	80.7	8.0	90.7	160.0	8.1	0.5	8.5	9
XS500B2		160.2	160.1	9.9	140.3	140.3	8.0	0.88	–	8.5
XS500B3		151.5	150.5	5.9	151.0	151.0	6.2	1	–	7.9
XS700B1	S700	120.6	120.5	8.1	51.0	153.8	6.1	0.42	6.1	6.5
XS700B2		151.9	200.0	9.8	80.9	100.7	4.2	0.53	5.8	6
XS700B3		141.8	181.0	5.3	120.3	80.8	6.1	0.85	–	6.8

Table 3
Welding details.

Welding company	Steel grade	Filler metal	f_y [MPa]	f_u [MPa]	A [%]	Min preheat [°C]	Max interpass [°C]	Heat input [kJ/mm]
Company A	S355	Carbofil 1	502	574	28	20	200	1–1.4
	S500	Union NiMoCr	720	780	17	20	200	1–1.4
	S700	Union NiMoCr	720	780	17	20	200	1–1.4
Company B	S355	MEGAFIL 710 M	551	609	24	20	150	0.4–1.0
	S500	MEGAFIL 710 M	551	609	24	50	135	0.8–1.5
	S700	MEGAFIL 742 M	763	790	20	50	100	0.6–1.1

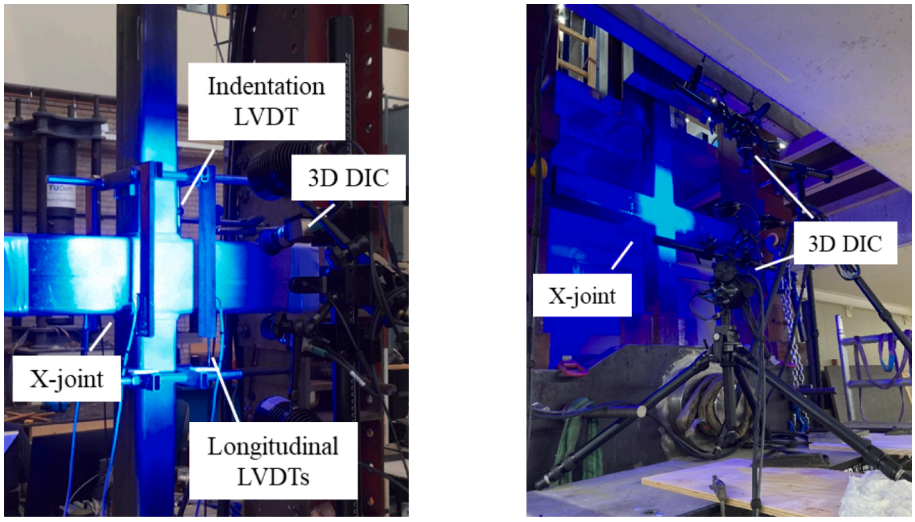

a) Setup with 2 MN capacity b) Setup with 10 MN capacity

Fig. 2. X-joint test setup.

Four Linear Variable Differential Transformers (LVDTs) were used to measure the longitudinal deformation of the A-series joints based on a $2b_0$ initial gauge length. An indentation LVDT was positioned at the centre line of the chord top surface to measure the chord top surface indentation, as shown in Fig. 1 and Fig. 2 a). The measuring point was 30 mm from the out surface of the brace. The base for holding the LVDT was 425 mm from the measuring point. Besides, the 3D digital image correlation (DIC) was used to measure the deformation of the specimen. The calibrated measuring volume was 350 mm × 280 mm × 280 mm with a maximum 0.05 pixel deviation. It was found that the results from

LVDT and DIC showed a good agreement. Therefore, the LVDTs were not used in the B-series testing.

2.2. Tensile coupon tests

Tensile coupon tests were conducted to obtain the mechanical property of RHS in X-joints. Coupon specimens were taken from the wall opposite the longitudinal weld of RHS, as shown in Fig. 3. Two specimens were symmetrically positioned around the symmetric axis of the tube with a distance (d), as summarised in Appendix A. In a companion work [27], it is found that the testing results of two symmetrically positioned specimens do not show any significant scattering. Hence, only two specimens were designed for each profile. According to ISO 6892–1 [28], a 5.65 proportional coefficient was used, resulting in a 50 mm initial gauge length and an 80 mm^2 cross-sectional area. The basic dimensions of the coupon specimen are presented in Fig. 4.

The measured thickness (t) and the width (b) are summarized in Appendix B. Note that the cross-sectional area of minor specimens was not 80 mm^2 but 50 mm initial gauge length was used for all coupons. The coupon specimen was only fabricated from the chords for the A-series joints. Since specimens XS355A3 and XS500A3 used the same profile for the chord and brace, the dimensions of the brace coupon specimen were the same as the chord. For other braces in A-series, the material property referred to other profiles with the same thickness as the brace and delivered as the same batch material. Besides, only one specimen was tested for the brace of XS355B3.

The tensile coupon test was carried out in an Instron testing machine with a 200 kN capacity. The loading controlled by the displacement was 0.01 mm/s, satisfying the loading rate requirement in [28]. The deformation was measured by two 3D DICs positioned perpendicular, as shown in Fig. 5. One DIC faced the side surface of the coupon specimen, while another DIC measured the convex surface of the specimen. The elongation of the specimen was extracted from DIC facing the side surface. Three virtual extensometers were created at three positions close to the concave side, close to the convex side, and at the centre, as shown in Fig. 6. Since an initial bow existed in the coupon specimen, the measured three deformations were averaged to obtain the elongation of the specimen. The measuring volume of two 3D DIC devices was 85 mm × 60 mm × 40 mm.

3. Testing results

3.1. Coupon test results

According to [29], the yield strength f_y (0.2 % proof stress), the ultimate strength f_u, the ultimate strain ε_u, and the elongation at failure ε_f are determined for each specimen and summarised in Appendix C. The stress–strain relationships are presented in Appendix D. Note that 'C' and 'B' in the name of the specimen represent 'chord' and 'brace', respectively.

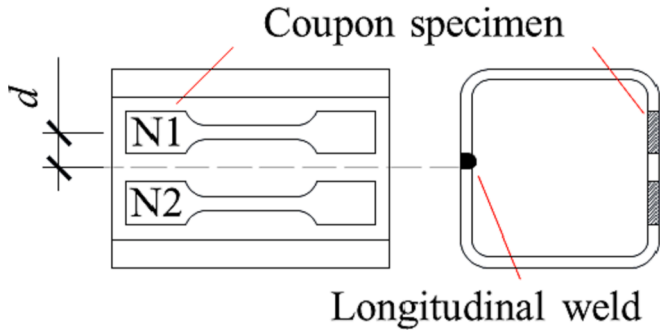

Fig. 3. Specimen cutting scheme.

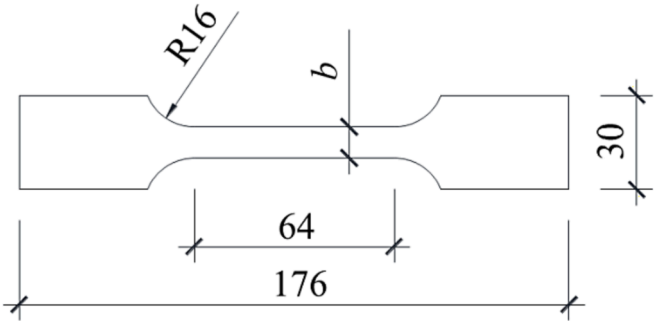

Fig. 4. Basic dimensions of coupon specimen [mm].

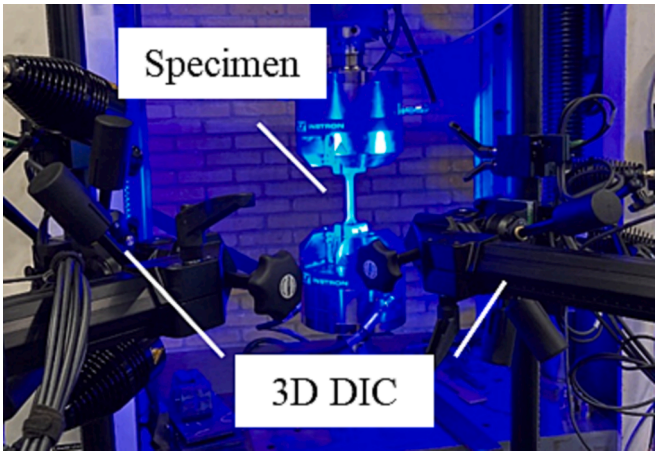

Fig. 5. Coupon test setup.

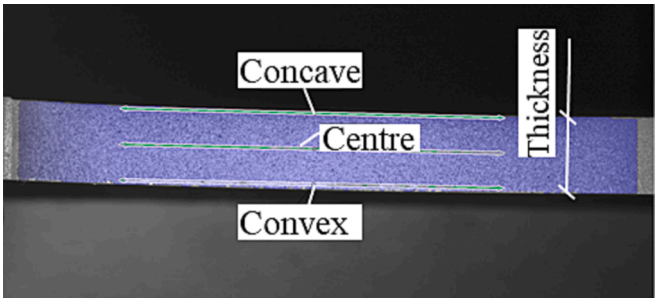

Fig. 6. Three virtual extensometers in DIC.

3.2. X-joint test results

All X-joints were broken at HAZ, either BF or PSF, except for XS355A3 with CSWF (for this joint, $\beta = 1$). The total deformation (D) of the joint was measured between two cross-sections with a $2b_0$ distance, see Fig. 1 and Fig. 2 a). The indentation of the chord surface was converted to a deformation ratio (D^*) by dividing the indentation by b_0 to trace the 3 %b_0 deformation limit. If the 3 %b_0 deformation limit was reached before the ultimate resistance (R_u), the joint failure was characterized as a combined failure mode of CFF and the failure mode corresponding to the final fracture, and the ultimate resistance was modified to the load at 3 %b_0 deformation ($R_{u\&3\%}$). If the 3 %b_0 deformation limit was not reached, $R_{u\&3\%}$ equals R_u.

The deformation measured by LVDTs and DIC was used for the A- and B-series specimens, respectively. Besides, the descending part corresponding to the final failure was missing for some of the load-deformation relationships presented in this section since 3D DIC could

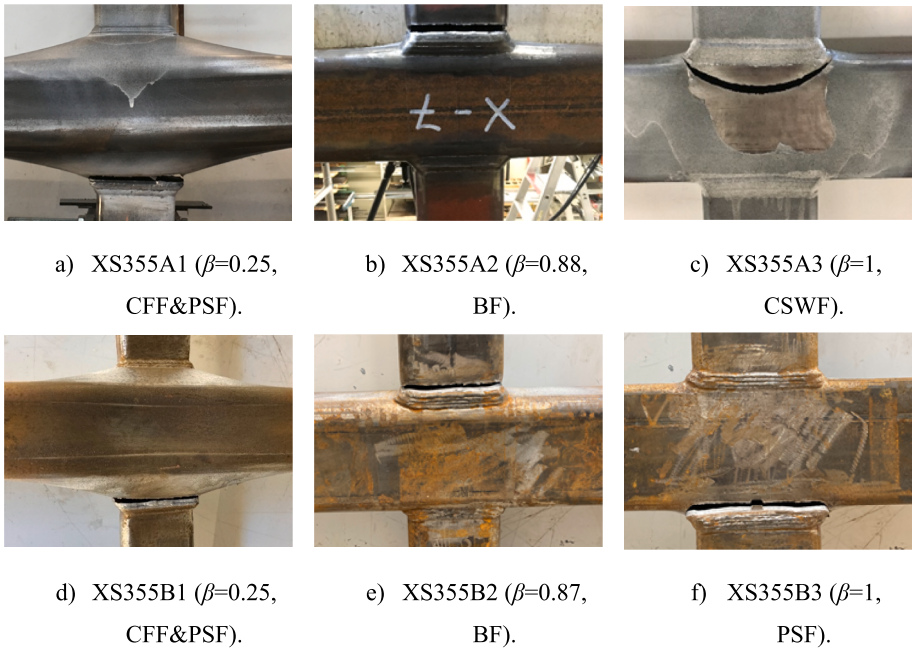

a) XS355A1 (β=0.25, CFF&PSF). b) XS355A2 (β=0.88, BF). c) XS355A3 (β=1, CSWF).

d) XS355B1 (β=0.25, CFF&PSF). e) XS355B2 (β=0.87, BF). f) XS355B3 (β=1, PSF).

Fig. 7. Failure modes of S355 X-joints.

not recognize the speckle pattern on the specimen after the final failure. Therefore, the last point in the curve is the moment just before the final failure.

3.2.1. S355 X-joints

Fig. 7 presents the failure mode of S355 joints. Due to the small β value, a profound chord face plastification appeared in XS355A/B1, which eventually failed in the chord. From Fig. 8 b), it can be seen that the 3 %b_0 deformation limit, highlighted in yellow, was reached at an early stage. Hence, the failure mode of XS355A/B1 was a combination of CFF and PSF. The load–displacement relationships of each configuration show good agreements. R_u, $R_{u\&3\%}$, and the failure mode are summarized in Table 4.

The 3 %b_0 deformation limit was not reached by specimens XS355A/B2 and XS355A/B3, although XS355A2 and XS355A3 were very close (see Fig. 8 b)). Hence, CFF did not appear in these four specimens. Both specimens with a moderate β (0.87 and 0.88) failed in the brace, while the specimens with $\beta = 1$ had different failure modes: CSWF and PSF for A-series and B-series, respectively. The ultimate resistance between the two series agreed well, with<5 % variation.

3.2.2. S500 X-joints

The chord width (b_0) used in XS500A1 was larger than that of XS500B1, while the dimension of the brace was kept the same. Consequently, the load at 3 %b_0 deformation for XS500B1 (589 kN) was higher than XS500A1 (428 kN), as shown in Fig. 10 b). Note that the LVDT measuring the chord face indentation of XS500A1 reached the maximum range at approximately 500 kN. Hence, the curve went straight up after 500 kN. Both specimens had a PSF, where a thorough fracture around the brace appeared in the chord of XS500A1 (Fig. 9 a)), and only one side of XS500B1 (Fig. 9 d)) failed. The ultimate loads of XS500A1 and XS500B1 were 897 kN and 887 kN, respectively. Besides, the stiffness at the plastic stage increased as the load was above 700 kN, indicating that the dominant mechanism changes from the chord face in bending to the chord face in tension which is so called the membrane effect.

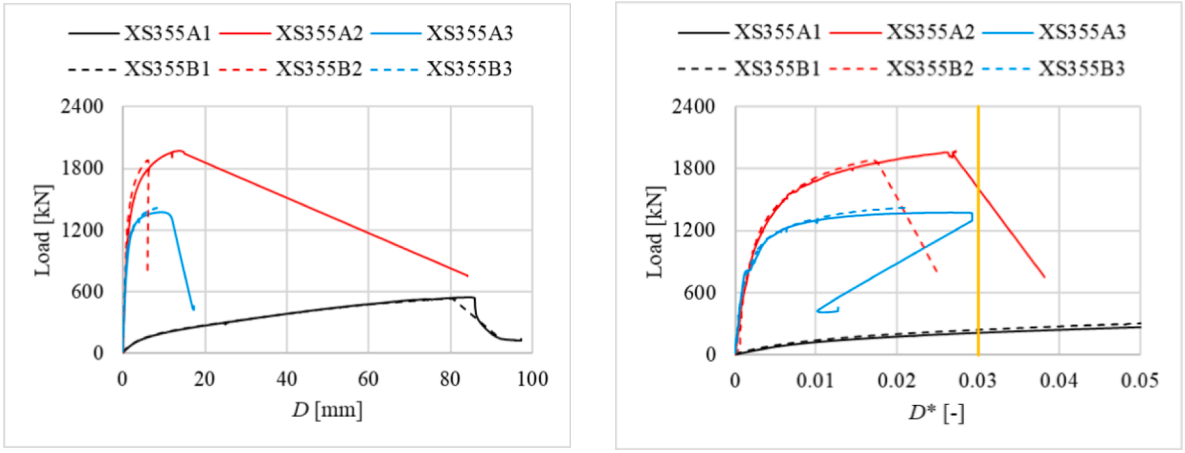

a) Total deformation. b) Chord face indentation ratio.

Fig. 8. Load-displacement relationship of S355 X-joints.

Table 4
X-joint test results.

Specimen	β	R_u [kN]	$R_{u\&3\%}$ [kN]	Failure mode	Specimen	β	R_u [kN]	$R_{u\&3\%}$ [kN]	Failure mode
XS355A1	0.25	546	215	CFF&PSF	XS355B1	0.25	532	240	CFF&PSF
XS355A2	0.88	1972	1972	BF	XS355B2	0.87	1883	1883	BF
XS355A3	1	1374	1374	CSWF	XS355B3	1	1424	1424	PSF
XS500A1	0.45	897	428	CFF&PSF	XS500B1	0.5	887	589	CFF&PSF
XS500A2	0.87	2213	2213	BF	XS500B2	0.88	1981	1981	PSF
XS500A3	1	1713	1713	BF	XS500B3	1	1557	1557	BF&PSF
XS700A1	0.42	890	852	CFF&PSF	XS700B1	0.42	1030	863	CFF&PSF
XS700A2	0.5	784	784	BF	XS700B2	0.53	788	788	BF
XS700A3	0.86	962	962	PSF	XS700B3	0.85	716	716	BF

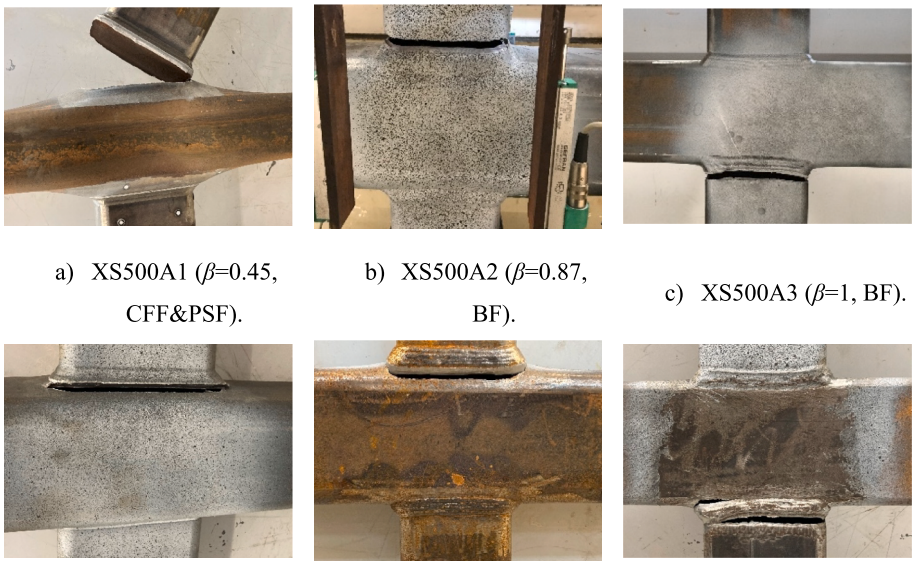

a) XS500A1 (β=0.45, CFF&PSF). b) XS500A2 (β=0.87, BF). c) XS500A3 (β=1, BF).

d) XS500B1 (β=0.5, CFF&PSF). e) XS500B2 (β=0.88, PSF). f) XS500B3 (β=1, BF&PSF).

Fig. 9. Failure modes of S500 X-joints.

Different failure modes, BF and PSF, were obtained from XS500A2 and XS500B2 (Fig. 9 b) and e)), respectively, although the dimensions of the members were the same. The ultimate loads of XS500A2 and XS500B2 were 2213 kN and 1976 kN, respectively. Fig. 10 a) shows that the ultimate resistance and the deformation capacity of XS500B2 were smaller than XS500A2. The same trend was observed in the specimens XS500A/B3. A possible reason for this difference is that the filler metal used in S500 B-series was much weaker than A-series, resulting in a softer HAZ in B-series, and consequently lower deformation and resistance.

Both specimens with $\beta = 1$ failed in the brace, as shown in Fig. 9 c) and f). In addition, a short fracture occurred at the corner of the chord in XS500B3, indicating that the resistance of BF and PSF was very close. The ultimate resistance of XS500A3 and XS500B3 was 1713 kN and 1557 kN, respectively. The 3 %b_0 deformation limit was not reached.

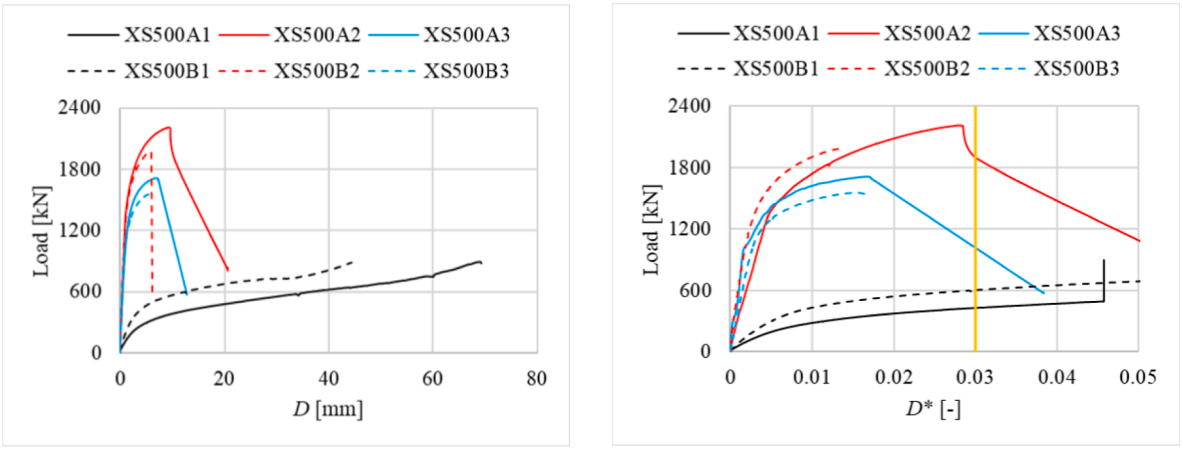

a) Total deformation. b) Chord face indentation ratio.

Fig. 10. Load-displacement relationship of S500 X-joints.

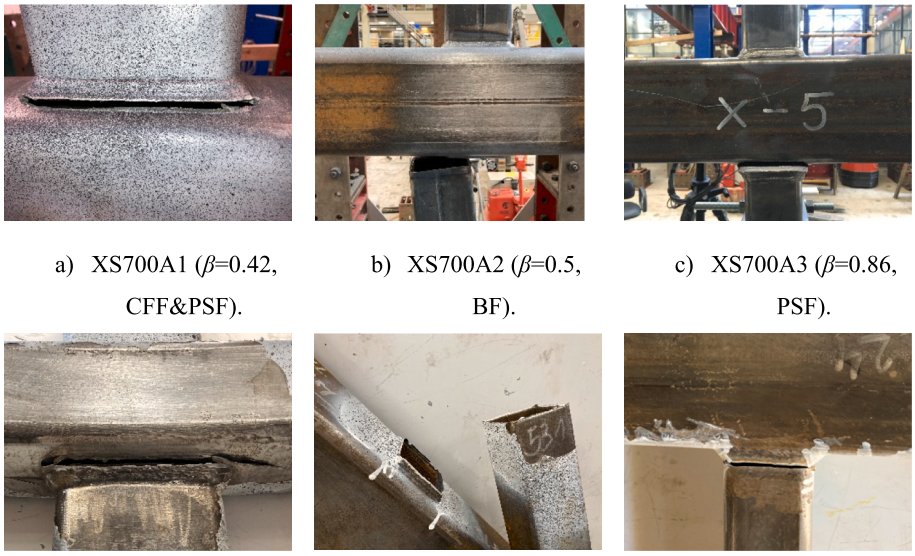

a) XS700A1 (β=0.42, CFF&PSF). b) XS700A2 (β=0.5, BF). c) XS700A3 (β=0.86, PSF).

d) XS700B1 (β=0.42, CFF&PSF). e) XS700B2 (β=0.53, BF). f) XS700B3 (β=0.85, BF).

Fig. 11. Failure modes of S700 X-joints.

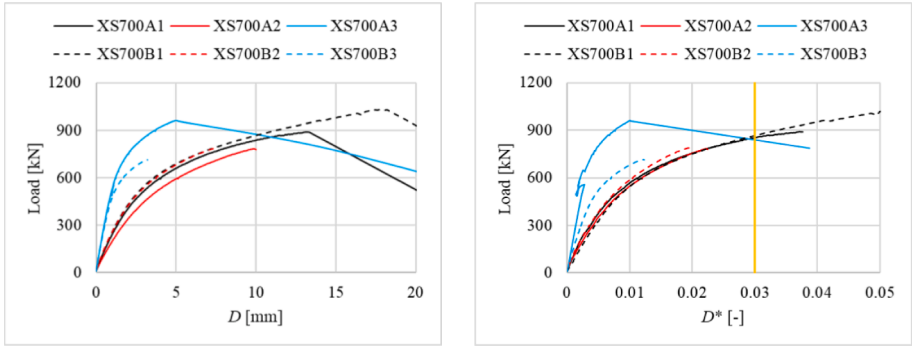

a) Total deformation. b) Chord face indentation ratio.

Fig. 12. Load-displacement relationship of S700 X-joints.

3.2.3. S700 X-joints

The same failure mode PSF was obtained from the specimens XS700A/B1, as shown in Fig. 11 a) and d). Fig. 12 demonstrates a good match between XS700A1 and XS700B1 before the 3 %b_0 deformation limit. Fig. 11 b) and e) present the failure mode (BF) of XS700A/B2. A thorough fracture involving the whole brace cross-section suddenly appeared at the end of testing. Neither specimen reached the deformation limit, as shown in Fig. 12 b). R_u, $R_{u\&3\%}$, and the failure mode are shown in Table 4.

Fig. 12 b) demonstrates that XS700A/B3 did not reach the 3 %b_0 deformation limit. Although the chord of XS700B3 was thinner than XS700A3, the failure mode transformed from PSF in XS700A3 to BF in XS700B3, as shown in Fig. 11 c) and f). And the resistance of XS700B3 (716 kN) was much lower than XS700A3 (962 kN). It indicates that the welding process, consequently the HAZ material property, has a crucial influence on the joint behaviour.

3.2.4. X-joints with different steel grades

As most of the specimens' dimensions among different steel grades are not identical, only two sets of specimens could be used to reveal the effect of the steel grade on the joint behaviour. The specimens XS355A/B2, XS500A/B2, and XS700A/B3 have a similar β value (around 0.87). The test results show that the ultimate deformation of S355 and S500 specimens is at least 0.014b_0, while S700 specimens have a deformation of around 0.01b_0. Similarly, with the same β value, XS700A2 has a significantly smaller ultimate deformation than XS500B1, indicating that the deformation capacity of the joint decreases with the increase of the steel grade. The explicit effect of the steel grade on the failure mode is not observed in the experiments. As the dimensions of the two sets of specimens vary, a direct comparison of the resistance is impossible.

4. Discussions

4.1. Characterization of the joint yield resistance

According to the design guide [30], the joint resistance is defined by the lower of the ultimate resistance and the load corresponding to the 3 %b_0 deformation limit (if reached). However, in an elasto-plastic global analysis, it is essential to describe the full-range behaviour of a joint using a simplified model, such as a bi-linear model in prEN 1993–1-8 [4].

Zanon and Zandonini [31] proposed a model for characterising the joint yield flexural resistance based on the initial and post-yielding stiffness, as shown in Fig. 13 a). It is straightforward to determine the initial stiffness using the linear part. However, the criterion for determining the post-yield stiffness is rather elusive. Different post-yielding part of the curve leads to different post-yielding stiffness, resulting in an arbitrary yield resistance. Lee et al. [24] appraised the joint ductility based on the equal energy criterion, see Fig. 13 b). The initial tangential stiffness line is used as a reference. A horizontal line is adjusted such that the two hatched blue areas are equal. The ratio D_2/D_1 is used to identify joint ductility. The nonlinear load-deformation relationship is converted to an equivalent elasto-plastic bi-linear model. However, the post-peak part is involved in the energy equilibrium. The energy consumed at the hardening stage is overestimated, resulting in an unconservative equivalent elasto-plastic behaviour. Moreover, the joint hardening behaviour cannot be recognized by Model 2.

Based on the aforementioned two models, a modified bi-linear model is proposed in this paper, as shown in Fig. 13 c). The initial stiffness line is the same as in the other two models. The horizontal plastic line in Model 2 is modified to an inclined line that ends at the ultimate resistance point. Shifting the intersection point of elastic and plastic lines, the two hatched blue areas vary. The yield resistance (R_y) is characterised by making the two areas equal. The advantages of the proposed model are primarily on properly addressing the following three aspects. First, a yield resistance is determined uniquely without a potential variation due to the "arbitrary" determined post-yielding stiffness. Second, a higher yield ratio (R_y/R_u) is rather correctly influenced by better ductility, e.g. higher D_2/D_1 ratio of a joint, as discussed in the next section. Third, the bi-linear model properly considers the post-yielding behaviour, which enables an adequate elasto-plastic global analysis.

4.2. Comparison of experimental and semi-analytical results

The yield and ultimate strength of each profile, shown in Appendix C, are averaged to calculate the joint resistance. C_f is derived for each yield strength according to Table 5 [4]. Table 6 presents the average yield strength of the chord (f_{y0}) and the brace (f_{y1}), the ultimate strength of the chord (f_{u0}) and the brace (f_{u1}), the modified yield strength of the chord ($f_{y0,M}$) and the brace ($f_{y1,M}$) according to the 0.8f_u restriction, and the corresponding C_f.

Table 5
Material factor C_f [4].

Yield strength range	Material factor C_f
$f_y \leq 355$ MPa	1.00
355 MPa $< f_y \leq$ 460 MPa	0.90
460 MPa $< f_y \leq$ 550 MPa	0.86
550 MPa $< f_y \leq$ 700 MPa	0.80

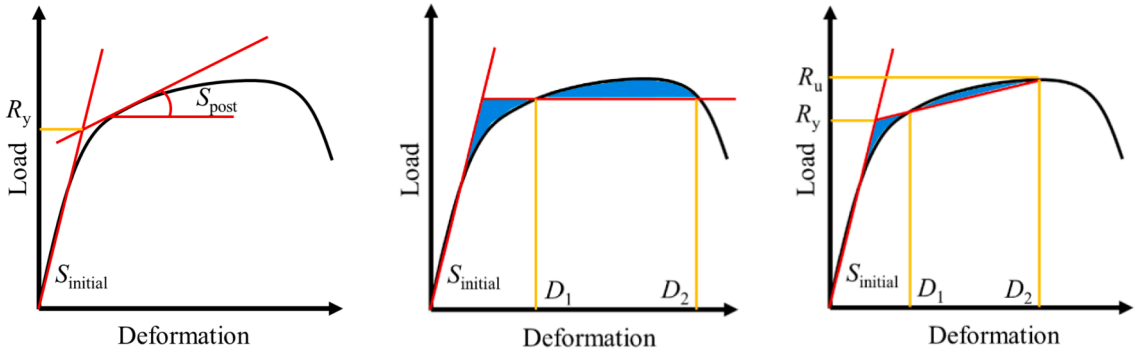

a) Model 1 [31] b) Model 2 [24] c) Model 3

Fig. 13. Bi-linear models.

Table 6
Average material strength and corresponding material factor.

Specimen	Chord					Brace			
	f_{y0} [MPa]	C_{f0}	f_{u0} [MPa]	$f_{y0,M}$ [MPa]	$C_{f0,M}$	f_{y1} [MPa]	f_{u1} [MPa]	$f_{y1,M}$ [MPa]	$C_{f1,M}$
XS355A1	522	0.86	553	442	0.90	505	543	434	0.90
XS355A2	486	0.86	516	412	0.90	506	532	425	0.90
XS355A3	452	0.90	510	408	0.90	452	510	408	0.90
XS500A1	558	0.80	597	477	0.86	580	612	489	0.86
XS500A2	589	0.80	624	499	0.86	580	612	489	0.86
XS500A3	609	0.80	670	536	0.86	609	670	536	0.86
XS700A1	751	0.80	846	677	0.80	780	861	689	0.80
XS700A2	726	0.80	831	665	0.80	741	848	678	0.80
XS700A3	780	0.80	861	689	0.80	780	861	689	0.80
XS355B1	519	0.86	549	439	0.90	546	590	472	0.86
XS355B2	499	0.86	532	425	0.90	530	547	438	0.90
XS355B3	484	0.86	523	419	0.90	484	523	419	0.90
XS500B1	598	0.80	634	507	0.86	550	584	467	0.86
XS500B2	573	0.80	617	493	0.86	617	648	518	0.86
XS500B3	596	0.80	646	516	0.86	596	646	516	0.86
XS700B1	783	0.80	861	689	0.80	792	867	693	0.80
XS700B2	743	0.80	808	647	0.80	741	848	678	0.80
XS700B3	722	0.80	825	660	0.80	784	864	691	0.80

Table 7
Results of the bi-linear model and prEN 1993-1-8 [4].

Specimen	Bi-linear model			prEN1993-1-8					
	R_y [kN]	$\frac{R_y}{R_u}$	$\frac{D_2}{D_1}$	R_{EC3} [kN]	Failure mode	$R_{EC3,non\text{-}cf}$ [kN]	Failure mode	$R_{EC3,non}$ [kN]	Failure mode
XS355A1	165	0.47	3.16	168	CFF	195	CFF	195	CFF
XS355A2	1563	0.79	3.41	1039	CFF&BF	1193	CFF&BF	1223	CFF&CSWF
XS355A3	1203	0.88	3.57	877	BF	974	BF	988	CSWF
XS500A1	357	0.52	3.75	233	CFF	291	CFF	291	CFF
XS500A2	1790	0.81	2.79	1090	CFF&BF	1343	CFF&BF	1379	CFF&CSWF
XS500A3	1388	0.81	2.91	1097	BF	1275	BF	1322	CSWF
XS700A1	605	0.68	2.49	357	CFF	446	CFF	446	CFF
XS700A2	501	0.64	2.14	467	CFF	583	CFF	583	CFF
XS700A3	707	0.74	2.37	421	CFF&BF	523	CFF&CSWF	523	CFF&CSWF
XS355B1	174	0.49	3.25	172	CFF	200	CFF	200	CFF
XS355B2	1448	0.77	2.88	1014	CFF&BF	1169	CFF&BF	1191	CFF&CSWF
XS355B3	1171	0.82	3.92	933	BF	1037	BF	1082	CSWF
XS500B1	540	0.74	2.77	283	CFF	354	CFF	354	CFF
XS500B2	1553	0.78	2.78	1140	CFF&BF	1395	CFF&BF	1428	CFF&CSWF
XS500B3	1235	0.79	2.86	1056	BF	1236	BF	1249	CSWF
XS700B1	662	0.64	2.90	391	CFF	489	CFF	489	CFF
XS700B2	508	0.64	2.20	495	CFF	619	CFF	619	CFF
XS700B3	525	0.73	2.21	286	CFF	357	CFF	357	CFF

4.2.1. General comparison

The results of the bi-linear model and the prEN 1993–1-8 [4] are presented in Table 7. The equations for predicting the X-joint tensile resistance are presented in Appendix D. R_y is the character yield resistance of the proposed bi-linear model (Model 3) in Section 4.1. Three design resistances are calculated, which consider a) C_f and the $0.8f_u$ restriction (R_{EC3}), b) the $0.8f_u$ restriction ($R_{EC3,non\text{-}Cf}$), and c) no restriction ($R_{EC3,non}$). Note that $R_{EC3,non\text{-}Cf}$ and $R_{EC3,non}$ are the same for the CFF and CSWF since the $0.8f_u$ restriction is not required for these two failure modes. The corresponding failure mode is also shown in the table. Since a linear interpolation is applied between the governing resistances at $\beta = 0.85$ and $\beta = 1$, a combined failure mode is presented for some joints.

Fig. 14 presents the varying range of $R_{EC3}/R_{u\&3\%}$ and $R_{EC3,non}/R_{u\&3\%}$ regarding the average yield strength for each steel grade. The average yield strength of S355, S500, and S700 are 498 MPa, 587 MPa, and 760 MPa, respectively. Since the β value of XS355A/B1 (0.25) is out of the valid geometry range in prEN 1993–1-8 [4] ($0.1 + 0.01b_0/t_0 = 0.35$), the resistance ratio is shown by the black point. Comparing R_{EC3} to $R_{u\&3\%}$, $R_{EC3}/R_{u\&3\%}$ of S355 and S500 joints varies in a similar range, as shown in Fig. 14 a). $R_{EC3}/R_{u\&3\%}$ of S700 joints is slightly lower than S355 and S500 joints. Note that the lower $R_{EC3}/R_{u\&3\%}$ of S700 joints does not mean the design rule for S700 joints is more conservative than S500 and S355 joints because the β value of tested specimens varies in different steel grades. Comparing Fig. 14 b) to a), the resistance ratio difference between S700 and S355/S500 slightly decreases without considering C_f and the $0.8f_u$ restriction. The maximum, average, and minimum resistance ratios are summarised in Table 8. The ratio excluding XS355A/B1 is presented in parentheses. Hence, a conclusion can be drawn that the design rule without using C_f and the $0.8f_u$ yield strength restriction predicts a conservative resistance. Note that this conclusion holds for all experimental studies of X-joints in tension presented in Table 1.

In addition, the joint nonlinear behaviour is characterised by the proposed bi-linear model. Note that the point where the post-yielding

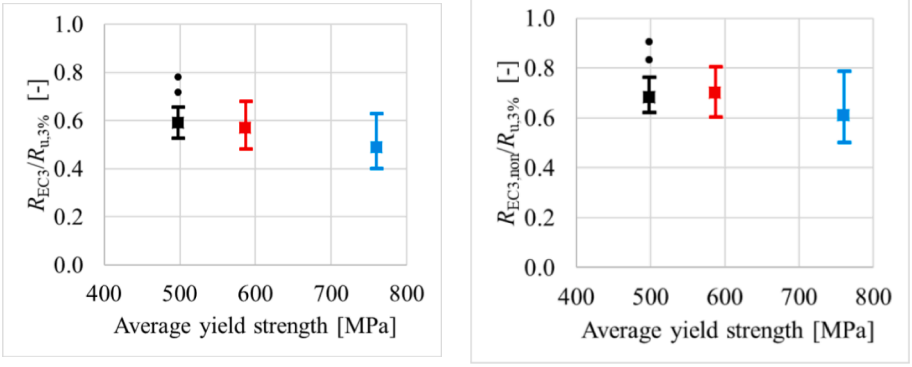

a) $R_{EC3}/R_{u\&3\%}$ b) $R_{EC3,non}/R_{u\&3\%}$

Fig. 14. Varying range of the resistance ratio.

Table 8
Range of resistance ratios.

Steel grade	Average f_y [MPa]	Type	$\frac{R_{EC3}}{R_{u\&3\%}}$	$\frac{R_{EC3,non}}{R_{u\&3\%}}$	$\frac{R_y}{R_u}$
S355		maximum	0.78 (0.66)	0.91 (0.76)	0.88
	498	average	0.64 (0.59)	0.75 (0.68)	0.70
		minimum	0.53	0.62	0.47
S500		maximum	0.68	0.80	0.81
	587	average	0.57	0.70	0.74
		minimum	0.48	0.60	0.52
S700		maximum	0.63	0.79	0.74
	760	average	0.49	0.61	0.68
		minimum	0.40	0.50	0.64

stiffness starts increasing is considered the ultimate resistance point of XS355A/B1 and XS500A/B1 since the membrane effect appeared. The yield ratio R_y/R_u varies between 0.47 and 0.88. For S355/S500 joints with $\beta < 0.5$, the ratio is around 0.5. For S355/S500 joints with $\beta \geq 0.5$ and S700 joints, the ratio is close to 0.7–0.8.

An example is presented in Fig. 15 a) to reveal the relationship between the joint ductility D_2/D_1 and the yield ratio R_y/R_u. The bi-linear model is characterised for two specimens with different ductility. Since the nominal dimensions of the two specimens are identical, the initial stiffness is the same. XS355A3 displays more ductile behaviour than XS500A3. $D_2/D_1 = 3.57$ and $R_y/R_u = 0.88$ for XS355A3 whereas $D_2/D_1 = 2.91$ and $R_y/R_u = 0.81$ for XS500A3. R_y/R_u is plotted against D_2/D_1 in Fig. 15 b), including all tested joints. In general, the better the joint ductility is, the higher the yield ratio is. Besides, D_2/D_1 and R_y/R_u decrease with the increase of the steel grade. Consequently, a larger safety margin (1-R_y/R_u) is obtained for joints made of HSS than for mild steel. Three joints (XS355A/B1 and XS500A1 with low β) show good ductility (above 3) but a rather conservative yield ratio (below 0.6) because the joints yielded at a very early stage and the deformation at the ultimate stage was substantially larger than other joints (see Fig. 8 and Fig. 10). Regardless of the low R_y/R_u, the three joints also demonstrate the same trend between D_2/D_1 and R_y/R_u as other joints.

4.2.2. Comparison of specific failure modes

Comparing Table 4 to Table 7, it can be seen that the failure mode of HSS joints is often mispredicted, which was also reported in the RUOSTE project [12]. Therefore, the resistance corresponding to the experimental failure mode is discussed in this section.

CFF is a dominant failure mode for tested joints with $\beta \leq 0.85$, as shown in Table 7. However, CFF was not observed in the experiments for XS700A2 ($\beta = 0.5$), XS700B2 ($\beta = 0.53$), and XS700B3 ($\beta = 0.85$), even though prEN 1993–1-8 predicts CFF to be the governing failure mode. The same phenomenon is observed in the RUOSTE project [12]. Two configurations of X-joints, namely TTX8 and TTX8W with $\beta = 0.67$, were made of S500, S700, and S960. CFF was predicted for all six joints, while BF was observed from two S960 and one S700 specimens. Besides these six joints, most of the joints had BF or PSF, while CFF was predicted. This discrepancy in the predicted and observed failure modes indicates that the design rule of prEN 1993–1-8 for X-joints in tension may need to be revised. One option might be the reduce the upper bound of β (0.85) for CFF as a function of steel grade. For joints with β between 0.85 and 1, the CFF resistance is used to determine the joint resistance by linear interpolation. Since CFF was not observed in the joints with $\beta > 0.85$, it might be reasonable to exclude CFF from the resistance determination.

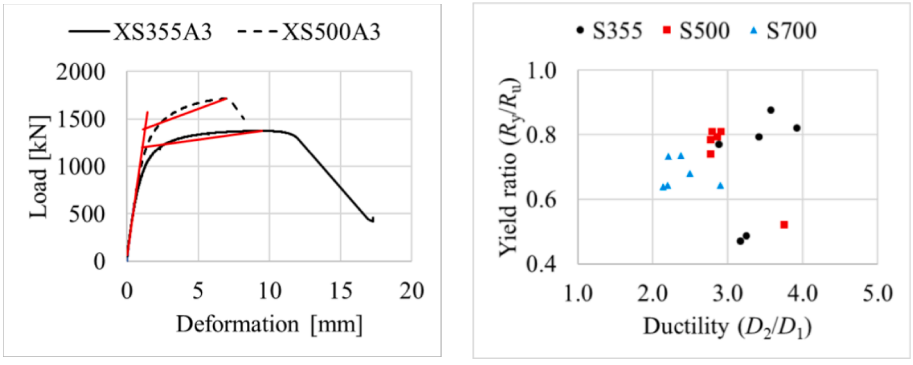

a) Example of joint characterisation b) Sum of all joints

Fig. 15. Relationship of the yield ratio and the ductility.

Table 9
Comparison of the resistance for the experimental failure mode.

Specimen	β	Experimental Failure mode	$R_{u\&3\%}$ [kN]	$R_{EC3,i}$ [kN]	$R_{EC3,i,non\text{-}Cf}$ [kN]	$R_{EC3,i,non}$ [kN]
XS355A1	0.25	CFF	215	168	195	195
XS355A2	0.88	BF	1972	1429	1588	1882
XS355A3	1	CSWF	1374	988	988	988
XS500A1	0.45	CFF	428	233	291	291
XS500A2	0.87	BF	2213	1556	1810	2137
XS500A3	1	BF	1713	1097	1275	1449
XS700A1	0.42	CFF	852	357	446	446
XS700A2	0.5	BF	784	766	958	1045
XS700A3	0.86	PSF	962	493	616	698
XS355B1	0.25	CFF	240	172	200	200
XS355B2	0.87	BF	1883	1449	1610	1920
XS355B3	1	PSF	1424	570	633	731
XS500B1	0.5	CFF	589	283	354	354
XS500B2	0.88	PSF	1981	1106	1286	1494
XS500B3	1	BF(PSF)	1557	1056(625)	1228(727)	1414(838)
XS700B1	0.42	CFF	863	391	489	489
XS700B2	0.53	BF	788	793	991	1082
XS700B3	0.85	BF	716	712	890	997

Besides, PSF appeared in joints with $\beta = 1$, which was also reported in [15–17], indicating that the upper bound of β which is 1–2 t_0/b_0 for PSF may need to be revised.

The resistances of the joints according to prEN 1993–1-8 corresponding to the experimental failure modes are summarised in Table 9. $R_{EC3,i}$, $R_{EC3,i,non\text{-}Cf}$, and $R_{EC3,i,non}$ are the predicted resistance considering a) C_f and the $0.8f_u$ restriction, b) the $0.8f_u$ restriction, and c) no restriction, respectively. The PSF resistance of XS500B3 is presented in parentheses.

$R_{EC3,i}$ and $R_{EC3,i,non}$ are compared to $R_{u\&3\%}$ in Fig. 16 for all 6 CFF joints. The resistance ratio is the predicted resistance ($R_{EC3,i}$ or $R_{EC3,i,non}$) over the experimental resistance ($R_{u\&3\%}$). The names in the legend, for example, 'S355' and 'S355,non', denote the ratio with and without considering C_f and the $0.8f_u$ restriction, respectively. Fig. 16 shows that all resistance ratio is below 1, including the joints out of the valid geometry range. Comparing S700 joints to S500 joints, the average $R_{EC3,i,non}/R_{u\&3\%}$ ratio decreases from 0.53 to 0.44, although the average elongation at failure of S700 material is 41 % lower than S500. The reduced material ductility has a limited influence on the conservative level of CFF prediction. In the literature, CFF of HSS X-joints in tension was only observed in the RUOSTE project [12], where the resistance ratio varies between 0.36 and 0.38 for joints up to S700 without using C_f and the $0.8f_u$ restriction. Hence, among the tested specimens in this study and literature, the material factor C_f is unnecessary among the tested specimens with CFF.

Besides, XS500A/B1 shows that the prediction is slightly more conservative with the increase of the β value, and XS700A/B1 shows that the prediction is less conservative with the rise of the material yield strength. These two observations align with the conclusion in [22,23]. With the increase of the steel grade, the elastic strain at yielding, f_y/E, increases. For example, the elastic strains at yielding of nominal S700 and S500 are 0.0035 and 0.0025, respectively, considering a 200GPa Young's Modulus. For a joint with a small β, the chord face bending dominates the deformation. Assuming the plane section remains plane at the plastic hinge, with the same 3 $\%b_0$ deformation, S700 and S500 plastic hinges are expected to have the same linear strain distribution through the thickness. Since S700 has a larger elastic strain at yielding, the material central layer remaining in the elastic stage is thicker, and the portion of the elastic strain over the total strain in the outer (yielding) layer is higher, compared to S500. Hence, the higher the steel grade is, the less the plastic deformation and the material strain hardening are. In addition, material strain hardening generally reduces with the rise of the steel grade. Therefore, with less material hardening at the same deformation, the resistance prediction is less conservation for

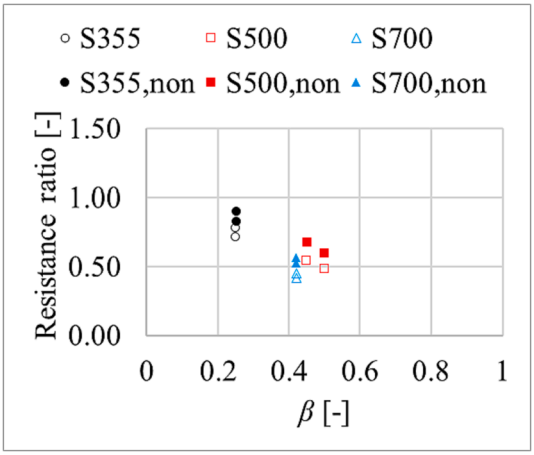

Fig. 16. Resistance ratio against β for CFF.

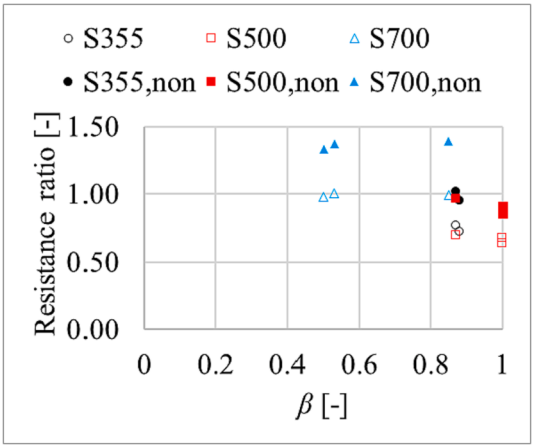

Fig. 17. Resistance ratio against β for BF.

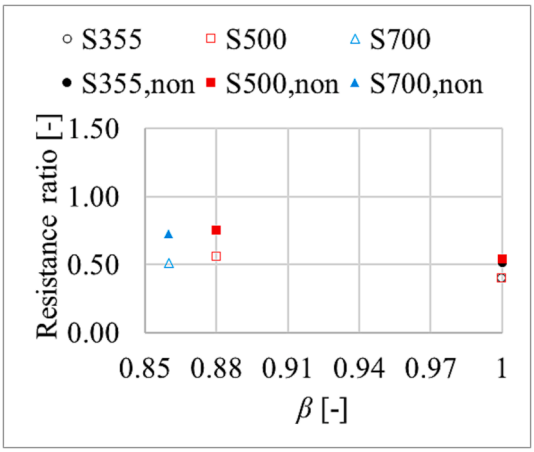

Fig. 18. Resistance ratio against β for PSF.

joints made of HSS and UHSS than mild steel. It might seem strange that the resistance ratio of S700 is lower than for S500, which seems against the trend explained above. This is due to the stronger material hardening behaviour of S700 than S500, as the average strength ratio (f_u/f_y) of S500 and S700 is 1.07 and 1.12, respectively.

8 joints failed with BF. $R_{EC3,i}/R_{u\&3\%}$ of S355 and S500 joints vary in a small range (0.64–0.77), averagely 0.75 and 0.67, respectively, as shown in Fig. 17. Without applying C_f, the varying range of the resistance ratio increases to 0.74–0.86 for S355 and S500 joints. And the range further increases to 0.85–1.02, if C_f and the $0.8f_u$ restriction are not applied. However, the $R_{EC3,i}/R_{u\&3\%}$ of S700 joints varies between 0.98 and 1.01. The average ratio is 1.37 if C_f and the $0.8f_u$ restriction are not applied. The reason for the prediction difference among different steel grades is that a more severe HAZ strength reduction was found in S700 material than in S500 and S355 material, as illustrated in [32,33]. Hence, the HAZ strength has a significant influence on the BF resistance. As the weld type could influence the shape of HAZ, consequently the resistance of BF, only the butt-welded X-joints in literature are included in this discussion. The resistance of four butt-welded X-joints made of C450 [17], S420 and S460 [16] with BF are safely predicted without using C_f. The resistance ratio varies between 0.73 and 0.88, which shows good agreement with the current experimental study. Therefore, among the tested specimens in this study and literature, C_f is not necessary for BF joints with steel grades up to S500, while the $0.8f_u$ restriction is needed for all steel grades.

The PSF resistance is substantially underestimated, especially for joints with $\beta = 1$, by design rules considering C_f and the $0.8f_u$ restriction, as $R_{EC3,i}/R_{u\&3\%}$ is generally below 0.57 among all steel grades, see Fig. 18. Relaxing C_f and the $0.8f_u$ restriction, the maximum resistance ratio increases to 0.75, which is still relatively low. Only one butt-welded X-joint with PSF is found in the literature [17]. The X-joint is made of C450 and the resistance ratio is 0.87 (without considering C_f and the $0.8f_u$ restriction). Hence, among the tested specimens in this study and literature, C_f and the $0.8f_u$ restriction could be relaxed for PSF for steel grades up to S700.

XS355A3 is the only specimen with CSWF, which has a 0.72 $R_{EC3,i}/R_{u\&3\%}$. C_f and the $0.8f_u$ restriction are not relevant for this failure mode.

To conclude, among the tested specimens in this paper and in the literature, the material factor C_f is not necessary for X-joints with a butt weld except for BF with S700 material. The $0.8f_u$ strength restriction can be relaxed for PSF but not for BF for butt-welded X-joints with steel grades up to S700. Although the prediction on PSF and CFF is conservative in general, it has to be emphasized that the weld type (butt weld or fillet weld) and the weld thickness have a significant influence on the joint resistance and stiffness, as illustrated in [26]. The tested specimen presented in this paper has the extra fillet weld due to the cap pass which may increase the ultimate resistance and stiffness of the joint. Hence, a further study should be carried out to investigate the effect of the weld type and the cap pass on the joint behaviour. Besides, BF and PSF highly depend on the HAZ strength. Since the HAZ strength reduction depends on the base material type and the welding parameters, it is essential to consider the HAZ strength reduction in the BF and PSF design.

5. Conclusions

The 18 tests on RHS X-joints in tension presented in this study, and a review of published results within the same area, provide additional insight into the requirement for the material factor C_f and the $0.8f_u$ restriction. The experiments of this study cover the steel grades S355J2H, S500MH, and S700MLH. The most relevant geometric parameters, β (the width ratio) and the member thickness, were varied in a wide range of values. For example, the β ratio had values between (and including) 0.25 and 1.0 such that all relevant failure modes could be obtained. The nominal chord and brace wall thickness ranged between 4 mm and 10 mm, which covers many practical design situations. In all specimens, the braces were connected to the chord by butt welds. The potential of quantified improvements of the joint resistance using fillet welds, rather common in practice and in the most of literature, is left out of the scope. The role of welding specifications (heat input, cooling time, etc.) should be explored further, especially for newer sorts of S500 and S700. The following key observations are highlighted:

1. The latest version of prEN 1993–1-8 predicts a conservative tensile resistance ($R_{EC3,non}$), for steel grade up to S700, even without applying C_f and the $0.8f_u$ restriction. This conclusion also holds for the X-joints tested in tension found in the literature, regardless of the weld type (butt weld or fillet weld). Comparing $R_{EC3,non}$ to $R_{u\&3\%}$ (the lower of the ultimate resistance (R_u) and the load at 3 %b_0 deformation), the maximum $R_{EC3,non}/R_{u\&3\%}$ is 0.8, excluding two S355 joints ($\beta = 0.25$, out of validated geometry range $0.1 + 0.01b_0/t_0 = 0.35$) which have a maximum of 0.91 $R_{EC3,non}/R_{u\&3\%}$.
2. Except for joints with chord face failure (CFF), prEN 1993–1-8 (2022) does not in general accurately predict the governing failure mode of the specimens presented in this paper and in the literature. The scope of the resistance expressions for the various failure modes should be explored further. For example, prEN 1993–1-8 predicts CFF in cases where it was not observed in the tests, especially for S700.
3. A modified bi-linear model is proposed to characterise the joint nonlinear behaviour and the yield resistance (R_y). The yield ratio R_y/R_u varies between 0.47 and 0.88. For S355/S500 joints with $\beta < 0.5$, the ratio is around 0.5. For S355/S500 joints with $\beta \geq 0.5$ and S700 joints, the ratio is close to 0.7–0.8. The better the joint ductility is, the higher the yield ratio is.

4. Regarding the predicted resistance corresponding to the experimental failure mode, it is found that C_f factor is not necessary except for the brace failure (BF) with S700 material. The $0.8f_u$ restriction could be relaxed for PSF but not for BF concerning steel grades up to S700. This conclusion holds for X-joints with a butt weld in this study and in the literature.
5. The material elongation at failure ε_f has a limited influence on the CFF resistance, but the material hardening behaviour does influence the CFF resistance. The material strength reduction in the heat-affected zone significantly affects the BF resistance.

The above observations and the results of the experiments lead to the following recommendations for updating the design rules for welded X-joints under tension loading in the braces:

1. The experimental results imply that the upper bound of β for CFF decreases with increasing steel grade, and the upper bound of β for punching shear failure (PSF) might not be necessary, regardless of the weld type (butt weld or fillet weld).
2. C_f and the $0.8f_u$ restriction are not necessary based on the current design rules, regardless of the mispredicted failure modes and the weld type.
3. For X-joints with a butt weld, if the failure mode is well predicted, C_f can be set to 1.0 for all failure modes for steel grades up to S700, except for BF for S700.
4. For X-joints with a butt weld, if the failure mode is well predicted, the $0.8f_u$ restriction can be neglected for all steel grades up to S700, except for BF for all steel grades.
5. As the heat-affected zone (HAZ) governs BF, a strength reduction factor for HAZ, especially for HSS and ultra-HSS, should be included in the formula of BF. Then, neither C_f nor the $0.8f_u$ restriction may be necessary for BF, regardless of the steel grade.

These recommendations are based on two experimental campaigns (18 experiments) and all available data in literature, and certainly more evidence obtained on modern steel types and welding technologies is needed to improve the competitiveness of welded joints in design standards.

CRediT authorship contribution statement

Rui Yan: Data curation, Formal analysis, Methodology, Investigation, Visualization, Writing – original draft, Writing – review & editing. **Kristo Mela:** Methodology, Writing – review & editing. **Hagar El Bamby:** Data curation, Writing - review & editing. **Milan Veljkovic:** Methodology, Supervision, Writing – review & editing.

Declaration of Competing Interest

The authors declare that they have no known competing financial interests or personal relationships that could have appeared to influence the work reported in this paper.

Data availability

Data will be made available on request.

Acknowledgements

The authors would like to thank the company SSAB Europe for the financial support for this research.

Appendix A. Nominal dimension of X-joints and position of coupon specimens.

Specimen	Steel grade	b_0 [mm]	h_0 [mm]	t_0 [mm]	d_0 [mm]	b_1 [mm]	h_1 [mm]	t_1 [mm]	d_1 [mm]
XS355A1	S355	200	100	8	20	50	100	5	20
XS355A2		160	160	10	25	140	140	8	25
XS355A3		150	150	6	20	150	150	6	20
XS500A1	S500	200	100	8	25	90	160	8	25
XS500A2		160	160	10	25	140	140	8	25
XS500A3		150	150	6	20	150	150	6	20
XS700A1	S700	120	120	8	20	51	152	6	25
XS700A2		160	160	10	25	80	100	4	20
XS700A3		140	140	6	25	120	80	6	25
XS355B1	S355	200	100	8	25	50	100	5	20
XS355B2		160	160	10	25	140	140	8	25
XS355B3		150	150	6	25	150	150	6	25
XS500B1	S500	180	80	8	25	90	160	8	25
XS500B2		160	160	10	25	140	140	8	25
XS500B3		150	150	6	25	150	150	6	25
XS700B1	S700	120	120	8	20	51	152	6	25
XS700B2		150	200	10	25	80	100	4	20
XS700B3		140	180	5	25	120	80	6	25

Appendix B. Measured dimensions of coupon specimens

Specimen	NO.	Chord [mm]		Brace [mm]		Specimen	NO.	Chord [mm]		Brace [mm]	
		t	b	t	b			t	b	t	b
XS355A1	N1	7.9	10.0	4.9	16.0	XS355B1	N1	7.9	10.2	5.1	16.2
	N2	7.8	10.0	4.9	16.0		N2	8.0	10.2	5.1	16.2
XS355A2	N1	9.8	7.8	8.1	10.0	XS355B2	N1	9.9	8.3	8.0	20.3
	N2	9.8	7.9	8.1	10.0		N2	9.9	8.1	8.1	20.2

(*continued on next page*)

(*continued*)

Specimen	NO.	Chord [mm]		Brace [mm]		Specimen	NO.	Chord [mm]		Brace [mm]	
		t	*b*	*t*	*b*			*t*	*b*	*t*	*b*
XS355A3	N1	6.0	13.0	6.0	13.0	XS355B3	N1	5.9	20.3	6.0	20.2
	N2	5.9	12.9	5.9	12.9		N2	6.0	20.2	–	–
XS500A1	N1	7.9	10.2	7.9	10.1	XS500B1	N1	7.9	10.2	7.8	13.3
	N2	7.8	10.1	7.9	10.0		N2	7.8	10.1	7.9	13.2
XS500A2	N1	9.8	7.8	7.9	10.1	XS500B2	N1	9.8	8.3	7.9	20.3
	N2	9.7	7.9	7.9	10.0		N2	9.9	8.1	7.9	20.2
XS500A3	N1	5.9	13.0	5.9	13.0	XS500B3	N1	6.0	20.2	6.0	20.2
	N2	5.9	13.0	5.9	13.0		N2	6.0	20.3	5.9	12.6
XS700A1	N1	7.9	10.3	5.8	13.3	XS700B1	N1	7.9	10.2	6.3	10.2
	N2	7.8	10.1	5.8	13.3		N2	8.0	10.1	6.4	10.2
XS700A2	N1	9.9	10.4	4.0	20.3	XS700B2	N1	9.4	8.4	4.0	20.3
	N2	9.8	8.3	4.0	20.2		N2	9.4	8.2	4.0	20.2
XS700A3	N1	5.8	13.3	5.8	13.3	XS700B3	N1	5.2	15.9	6.0	13.2
	N2	5.8	13.3	5.8	13.3		N2	5.2	16.4	5.9	13.2

Appendix C. Coupon test results

Specimen	NO.	Chord				Brace			
		f_y [MPa]	f_u [MPa]	ε_u [%]	ε_f [%]	f_y [MPa]	f_u [MPa]	ε_u [%]	ε_f [%]
XS355A1	N1	528	552	7.0	26.0	510	539	8.8	23.3
	N2	516	553	10.5	27.3	499	546	5.0	25.3
XS355A2	N1	477	515	9.5	27.2	504	535	8.1	26.9
	N2	495	516	10.3	30.6	508	528	8.1	26.6
XS355A3	N1	461	510	12.5	28.2	461	510	12.5	28.2
	N2	442	509	13.4	29.3	442	509	13.4	29.3
XS500A1	N1	571	603	1.6	22.3	575	609	5.2	24.8
	N2	544	590	5.2	24.6	585	614	1.9	24.9
XS500A2	N1	600	631	1.3	20.3	575	609	5.2	24.8
	N2	578	617	2.6	20.5	585	614	1.9	24.9
XS500A3	N1	612	671	6.9	22.9	612	671	6.9	22.9
	N2	605	668	8.4	24.1	605	668	8.4	24.1
XS700A1	N1	734	853	2.7	12.8	781	858	3.6	12.0
	N2	768	839	1.8	12.5	779	864	3.1	13.1
XS700A2	N1	710	836	2.9	17.3	740	850	3.5	10.1
	N2	742	826	1.9	12.5	741	846	3.3	10.4
XS700A3	N1	781	858	3.6	12.0	781	858	3.6	12.0
	N2	779	864	3.1	13.1	779	864	3.1	13.1
XS355B1	N1	506	545	11.9	27.7	551	590	1.5	18.2
	N2	532	552	10.5	26.8	541	590	1.3	17.8
XS355B2	N1	501	535	1.3	26.7	524	547	1.6	29.7
	N2	496	528	7.8	27.9	535	547	1.8	27.3
XS355B3	N1	471	520	13.6	29.3	487	524	11.3	29.2
	N2	493	526	12.2	29.0	–	–	–	–
XS500B1	N1	593	629	1.7	19.5	541	574	1.9	23.8
	N2	603	639	1.7	19.5	558	593	1.2	18.7
XS500B2	N1	574	610	1.7	19.7	609	648	1.4	19.8
	N2	572	623	1.3	19.8	624	648	1.2	18.7
XS500B3	N1	595	644	7.5	22.8	598	643	6.9	23.2
	N2	580	638	9.0	24.3	610	657	6.0	21.2
XS700B1	N1	773	855	2.4	14.4	791	864	2.9	12.5
	N2	792	867	2.0	13.5	792	869	2.7	12.7
XS700B2	N1	745	808	3.1	17.5	740	850	3.5	10.1
	N2	741	808	3.1	16.8	741	846	3.3	10.4
XS700B3	N1	720	823	4.9	13.5	777	860	2.2	12.1
	N2	724	827	4.7	15.6	791	867	2.2	12.7

Appendix D. Stress-strain relationships of tested coupon specimens

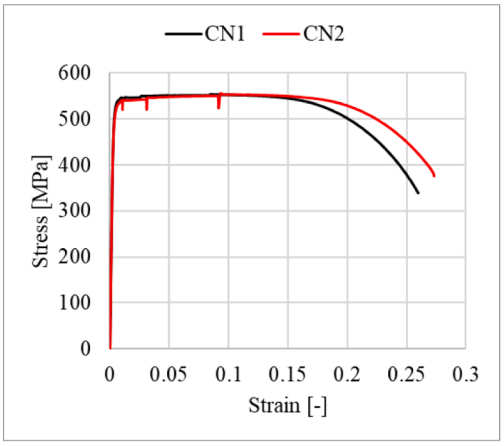

a) XS355A1

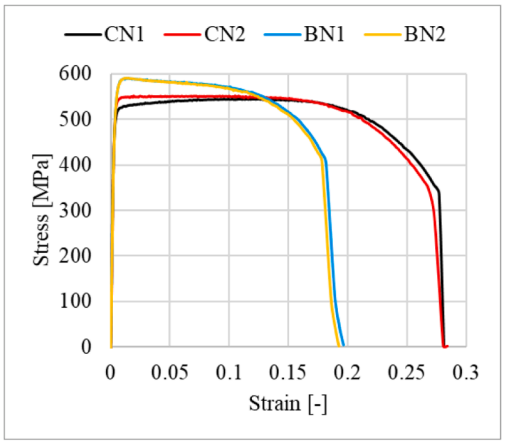

b) XS355B1

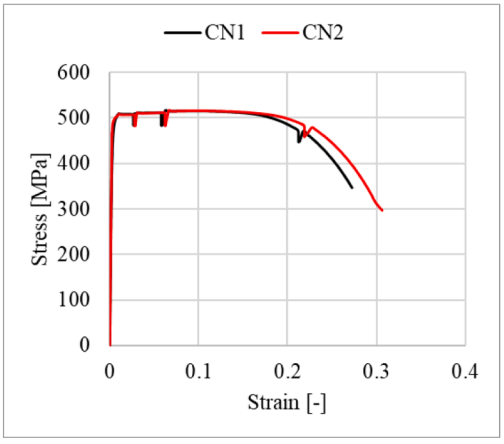

c) XS355A2

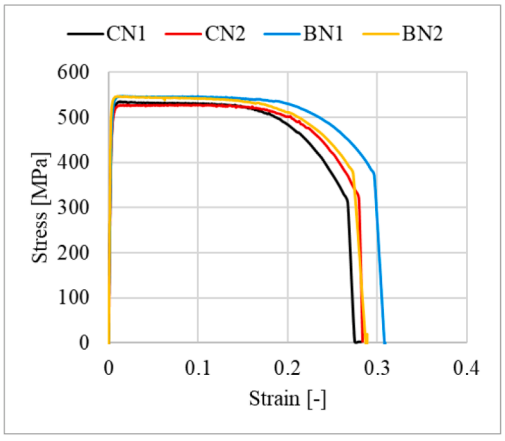

d) XS355B2

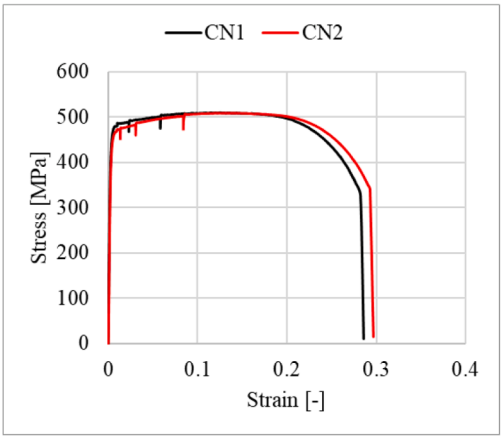

e) XS355A3

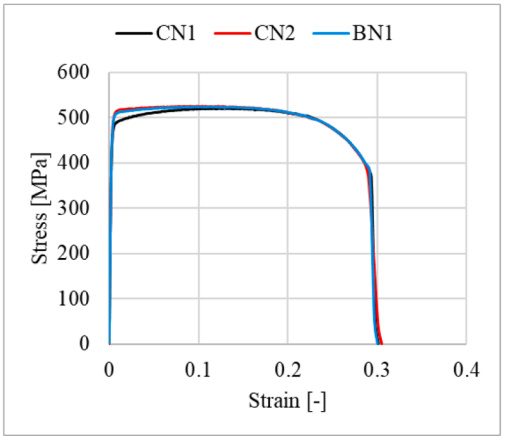

f) XS355B3

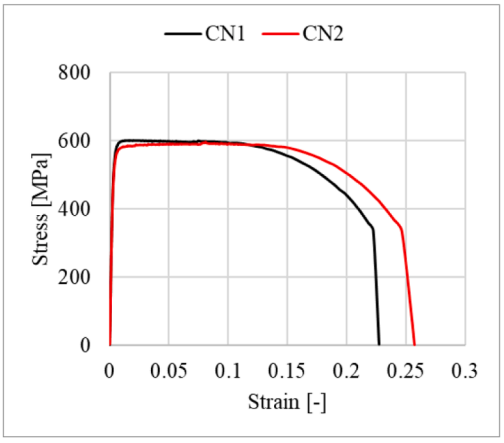

g) XS500A1

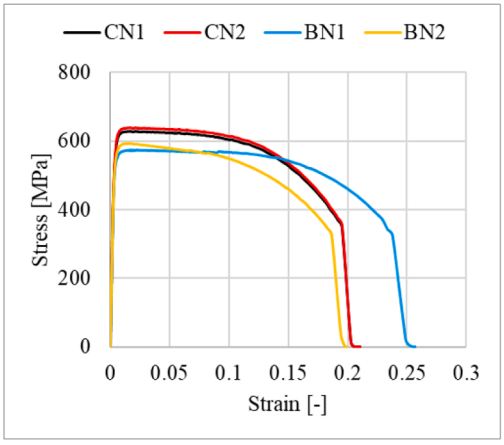

h) XS500B1

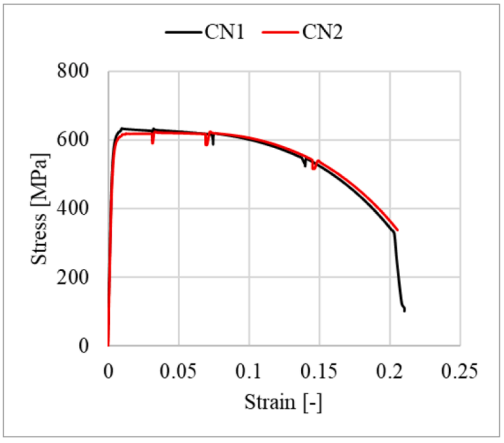

i) XS500A2

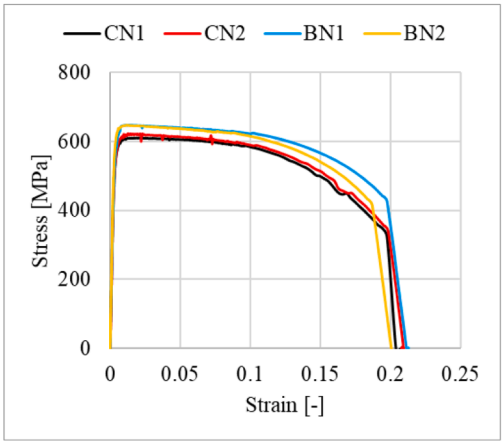

j) XS500B2

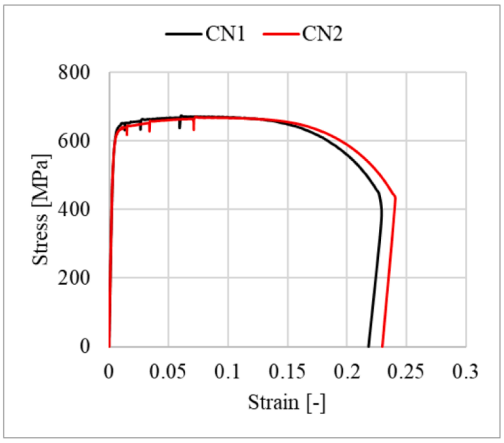

k) XS500A3

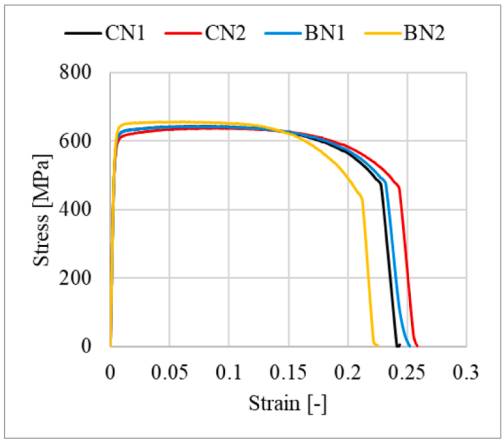

l) XS500B3

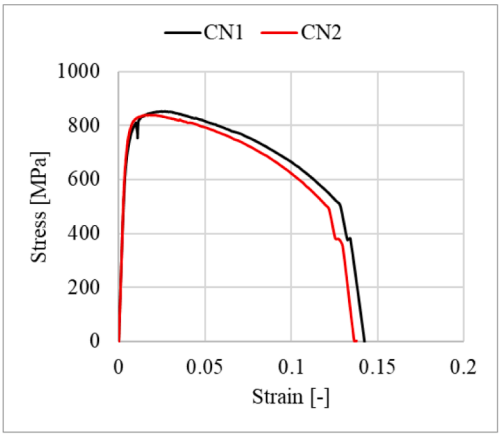

m) XS700A1

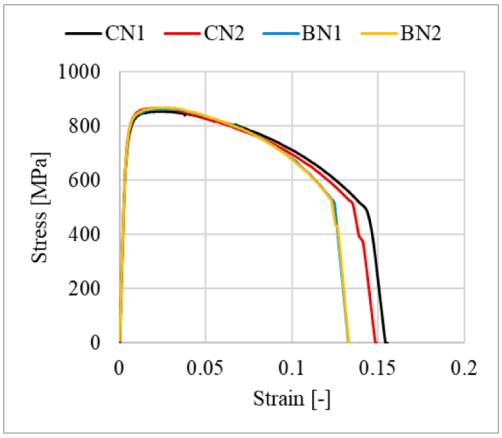

n) XS700B1

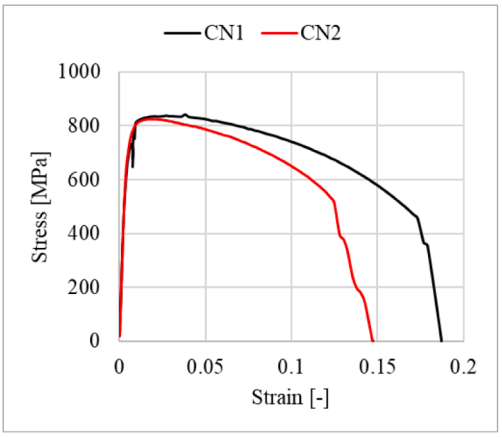

o) XS700A2

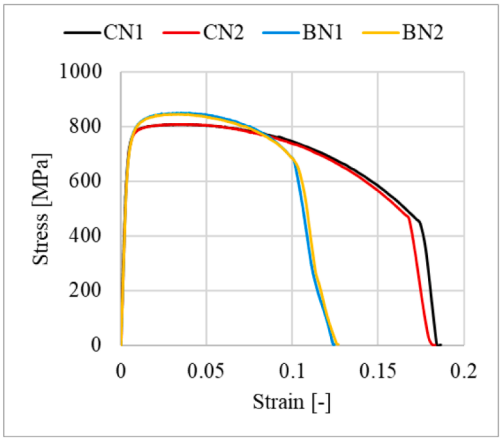

p) XS700B2

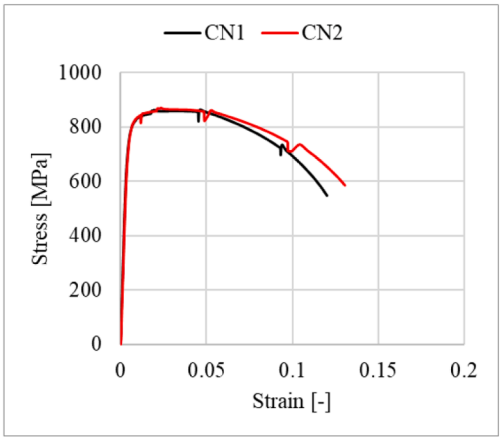

q) XS700A3

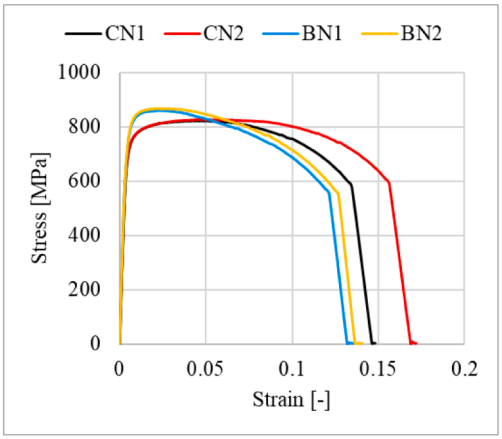

r) XS700B3

Appendix E. Design equations in prEN 1993-1-8 for X-joints in tension.

Failure mode	Equations
CFF $\beta \leq 0.85$	$N_{1,\mathrm{Rd}} = C_\mathrm{f}\frac{f_{y0}t_0^2}{\sin\theta_1}\left(\frac{2\eta}{(1-\beta)\sin\theta_1}+\frac{4}{\sqrt{1-\beta}}\right)\frac{Q_\mathrm{f}}{\gamma_{M5}}$
CSWF $\beta = 1.0$	$N_{1,\mathrm{Rd}} = \frac{f_\mathrm{b}t_0}{\sin\theta_1}\left(\frac{2h_1}{\sin\theta_1}+10t_0\right)\frac{Q_\mathrm{f}}{\gamma_{M5}}$

(continued on next page)

(*continued*)

Failure mode	Equations
BF	$N_{1,Rd} = C_f f_{y1} t_1 (2h_1 - 4t_1 + 2b_{eff}) \frac{1}{\gamma_{M5}}$ $b_{eff} = \min\left(\frac{10t_0}{b_0}\frac{f_{y0}t_0}{f_{y1}t_1}b_1, b_1\right)$
PSF $b_1 \leq b_0 - 2\,t_0$	$N_{1,Rd} = C_f \frac{f_{y0}t_0}{\sqrt{3}\sin\theta_1}\left(\frac{2h_1}{\sin\theta_1} + 2b_{e,p}\right)\frac{1}{\gamma_{M5}}$ $b_{e,p} = \min\left(\frac{10t_0}{b_0}b_1, b_1\right)$

where θ_1 is the angle between the brace and the chord ($\theta_1 = 90^\circ$ for the tested specimens), Q_f is the chord stress factor ($Q_f = 1$ for the tested specimens). For $0.85 < \beta < 1.0$ linear interpolation may be applied between the governing resistances as $\beta = 0.85$ (CFF,BF, and PSF) and $\beta = 1$ (CSWF and BF).

References

[1] EN 1993-1-8:2005 - Design of steel structures - Part 1-8: Design of joints; 2005.
[2] Molybdenum in Architecture, Building and Construction, Friends Arena, Stockholm; 2013. imoa.info/download_files/sustainability/IMOA_FriendsArena_12.pdf.
[3] EN 1993-1-12:2007 - design of steel structures - part 1–12: additional rules for the extension of EN 1993 up to steel grades S700; 2007.
[4] prEN 1993-1-8:2021 - Design of steel structures - Part 1-8: Design of joints (draft of EN1993-1-8: 2021); 2022.
[5] Kurobane Y. New developments and practices in tubular joint design, in: IIW Doc. XV-488-81 and IIW Doc. XIII-1004-81; 1981.
[6] Liu DK, Wardenier J. Effect of the yield strength on the static strength of uniplanar K-joints in RHS (steel grades S460, S355 and S235). In: IIW Doc. XV-E-04-293; 2004.
[7] Mang F. Untersuchungen an Verbindungen von geschlossenen und offenen Profilen aus hochfesten Stählen, Abschlussbericht AIF; 1978.
[8] Noordhoek C, Verheul A, Foeken RJ, Bolt HM, Wicks PJ. Static strength of high strength steel tubular joints, CIDECT Rep. 5BD-9/98; 1998.
[9] Stroetmann R, Kästner T, Hälsig A, Mayr P. Influence of the cooling time on the mechanical properties of welded HSS-joints. Steel Construct 2018;11:264–71. https://doi.org/10.1002/stco.201800019.
[10] Amraei M, Ahola A, Afkhami S, Björk T, Heidarpour A, Zhao X-L. Effects of heat input on the mechanical properties of butt-welded high and ultra-high strength steels. Eng Struct 2019;198:109460.
[11] Yan R, El Bamby H, Veljkovic M, Xin H, Yang F. A method for identifying the boundary of regions in welded coupon specimens using digital image correlation. Mater Des 2021;210:110073. https://doi.org/10.1016/j.matdes.2021.110073.
[12] Feldmann M, Schillo N, Schaffrath S, Virdi K, Björk T, Tuominen N et al., Rules on high strength steel; 2016. https://op.europa.eu/en/publication-detail/-/publication/515285b0-c820-11e6-a6db-01aa75ed71a1/language-en/format-PDF/source-194823584.
[13] Javidan F, Heidarpour A, Zhao XL, Hutchinson CR, Minkkinen J. Effect of weld on the mechanical properties of high strength and ultra-high strength steel tubes in fabricated hybrid sections. Eng Struct 2016;118:16–27. https://doi.org/10.1016/j.engstruct.2016.03.046.
[14] prEN 1993-1-12:2021 - Design of steel structures - Part 1-12: Additional rules for steel grades up to S960; 2021.
[15] Björk T, Saastamoinen H. Capacity of CFRHS X-joints made of double-grade S420 steel, Tubular Structures XIV - Proceedings of the 14th International Symposium on Tubular Structures, ISTS 2012; 2012 167–176. https://doi.org/10.1201/b13139-26.
[16] Tuominen N, Björk T. Capacity of RHS-joints made of high strength steels, CIDECT Report 5BZ, Final report; 2017.
[17] Becque J, Wilkinson T. The capacity of grade C450 cold-formed rectangular hollow section T and X connections: An experimental investigation. J Constr Steel Res 2017;133:345–59. https://doi.org/10.1016/j.jcsr.2017.02.032.
[18] Wardenier J, Lan X, Packer JA. Re-analysis of full-width RHS T- and X-joints under brace axial tension and brace in-plane bending; 2021.
[19] Pandey M, Young B. Compression capacities of cold-formed high strength steel tubular T-joints. J Constr Steel Res 2019;162:105650. https://doi.org/10.1016/j.jcsr.2019.05.040.
[20] Kim J-H, Lee C-H, Kim S-H, Han K-H. Experimental and Analytical Study of High-Strength Steel RHS X-Joints under Axial Compression. J Struct Eng 2019;145:04019148. https://doi.org/10.1061/(asce)st.1943-541x.0002435.
[21] Pandey M, Young B. Structural performance of cold-formed high strength steel tubular X-Joints under brace axial compression. Eng Struct 2020;208:109768. https://doi.org/10.1016/j.engstruct.2019.109768.
[22] Lan X, Chan TM, Young B. Structural behaviour and design of high strength steel RHS X-joints. Eng Struct 2019;200:109494. https://doi.org/10.1016/j.engstruct.2019.109494.
[23] Lan X, Chan TM, Young B. Testing, finite element analysis and design of high strength steel RHS T-joints. Eng Struct 2021;227:111184. https://doi.org/10.1016/j.engstruct.2020.111184.
[24] Lee C-H, Kim S-H, Chung D-H, Kim D-K, Kim J-W. Experimental and Numerical Study of Cold-Formed High-Strength Steel CHS X-Joints. J. Struct. Eng. 2017;143:04017077. https://doi.org/10.1061/(asce)st.1943-541x.0001806.
[25] Lee C-H, Kim S-H. Structural performance of CHS X-joints fabricated from high-strength steel; 2018. https://doi.org/10.1002/stco.201800021.
[26] Havula J, Garifullin M, Heinisuo M, Mela K, Pajunen S. Moment-rotation behavior of welded tubular high strength steel T joint. Eng Struct 2018;172:523–37. https://doi.org/10.1016/j.engstruct.2018.06.029.
[27] Yan R, Mela K, Yang F, El Bamby H, Veljkovic M. Equivalent material properties of the heat-affected zone in welded cold-formed rectangular hollow section connections (under review). Thin-Walled Struct 2022.
[28] Metallic materials - Tensile testing - Part 1: Method of test at room temperature (ISO 6892-1:2019) 2019;1.
[29] EN 1993-1-1:2005 - Design of steel structures - Part 1-1: General rules and rules for buildings; 2005.
[30] Packer J, Wardenier J, Zhao X, Van der veget G, Kurobane Y. Design guide for rectangular hollow section (RHS) joints under predominantly static loading (2nd ed); 2009.
[31] Zanon P, Zandonini R. Experimental analysis of end plate connections. In: Proceedings of the State of the Art Workshop on Connections and the Behaviour of Strength and Design of Steel Structures, Cachan; 1988. p. 41–51.
[32] Yan R, Xin H, Yang F, El Bamby H, Veljkovic M, Mela K. A method for determining the constitutive model of the heat-affected zone using digital image correlation. Constr Build Mater 2022;342:127981.
[33] Yan R, El Bamby H, Veljkovic M. Experimental and numerical study of butt welded joints made of high strength steel. In: The Eighth International Conference on Structural Engineering, Mechanics and Computation; 2022.